D. D. Girton T. R. Hawkinson L. F. Greimann
with K. Bergenson, U. Ndon, and R. E. Abendroth

Validation of Design Recommendations for Integral Abutment Piles

Sponsored by the Iowa Department of Transportation, Highway Division, and the Iowa Highway Research Board

September 1989
Iowa DOT Project HR-292

Iowa Department of Transportation

report

College of Engineering
Iowa State University

The opinions, findings, and conclusions expressed in this publication are those of the authors and not necessarily those of the Highway Division of the Iowa Department of Transportation.

D. D. Girton T. R. Hawkinson L. F. Greimann
with K. Bergenson, U. Ndon, and R. E. Abendroth

Validation of Design Recommendations for Integral Abutment Piles

Sponsored by the Iowa Department of Transportation, Highway Division, and the Iowa Highway Research Board

September 1989
Iowa DOT Project HR-292

engineering research institute
iowa state university

TABLE OF CONTENTS

LIST OF FIGURES

LIST OF TABLES

PREFACE

We are deeply grateful for the work of the late Professor Darrel D. Girton, who initiated this project on the displacements of integral abutment bridges. Professor Girton planned the entire project, did most of the field work at the two bridge sites, and developed the bridge displacement equation presented in Chapter 3. This final report is dedicated to the memory of Darrel D. Girton for his timely assistance before he passed away during the writing of this report.

Our special thanks for the contributions of Professor Ken Bergeson and his graduate assistant, Udeme Ndon, who determined the design coefficient of thermal expansion for the concrete at the two bridge sites.

We also want to thank Professor Robert E. Abendroth for his contributions to the design recommendations summarized in Chapter 5, as well as for his suggestions for the remainder of the report.

ABSTRACT

Since integral abutment bridges decrease the initial and maintenance costs of bridges, they provide an attractive alternative for bridge designers. The objective of this project is to develop rational and experimentally verified design recommendations for these bridges.

Field testing consisted of instrumenting two bridges in Iowa to monitor air and bridge temperatures, bridge displacements, and pile strains. Core samples were also collected to determine coefficients of thermal expansion for the two bridges. Design values for the coefficient of thermal expansion of concrete are recommended, as well as revised temperature ranges for the deck and girders of steel and concrete bridges.

A girder extension model is developed to predict the longitudinal bridge displacements caused by changing bridge temperatures. Abutment rotations and passive soil pressures behind the abutment were neglected. The model is subdivided into segments that have uniform temperatures, coefficients of expansion, and moduli of elasticity. Weak axis pile strains were predicted using a fixed-head model. The pile is idealized as an equivalent cantilever with a length determined by the surrounding soil conditions and pile properties. Both the girder extension model and the fixed-head model are conservative for design purposes.

A longitudinal frame model is developed to account for abutment rotations. The frame model better predicts both the longitudinal displacement and weak axis pile strains than do the simpler models. A lateral frame model is presented to predict the lateral motion of skewed bridges and the associated strong axis pile strains. Full passive soil pressure is assumed on the abutment face.

Two alternatives for the pile design are presented. Alternative One is the more conservative and includes thermally induced stresses. Alternative Two neglects thermally induced stresses but allows for the partial formation of plastic hinges (inelastic redistribution of forces). Ductility criteria are presented for this alternative. Both alternatives are illustrated in a design example.

NOMENCLATURE

b_f	flange width
c	distance from neutral axis to desired strain location
d	section depth
d_g	depth to strain gages below bottom of abutment
f_a	total, applied axial stress
f_{aT}	temperature-induced axial stress
f_{aV}	vertical-load axial stress
$f_{bx,y}$	total, applied bending stress about x,y
$f_{bx,yT}$	temperature-induced bending stress about x,y axis
$f_{bx,yV}$	vertical-load bending stress about x,y axis
f_A	correction factor for age
f_M	correction factor for moisture
f_T	correction factor for exposure condition
k_e	effective soil stiffness
k_h	initial, lateral soil stiffness
ℓ	total length of embedded pile
ℓ_c	critical length parameter
ℓ_e	equivalent length
ℓ_{eb}	equivalent embedment length for elastic pile buckling
ℓ_{eh}	equivalent embedment length for horizontal stiffness
ℓ_{em}	equivalent embedment length for maximum moment
ℓ_n	frictional length
ℓ_u	length of exposed pile above soil surface
$r_{x,y}$	radius of gyration about x,y axis
t_f	flange thickness
A_i	segmental area
B	skewed abutment width
C_i	inelastic, rotational capacity-reduction factor
$C_{mx,y}$	coefficient applied to bending term in interaction formula
E	modulus of elasticity
E_j	segmental modulus of elasticity
F_a	allowable axial stress

$\Delta_{ix,y}$	allowable total displacement consistent with inelastic rotation capacity
Δ_j	unrestrained displacement of segment j
$\Delta_{ox,y}$	lateral displacement
Δ_s	displacement of spring
Δ_w	displacement of wire
ΔT	temperature change
ΔT_j	temperature change for segment j
ε_i	strain gage number i
ε_a	axial strain
ε_t	strain due to torsional bending
ε_x	strain due to x,y axis bending
μ	coefficient of friction between soil and abutment
σ	normal stress

1. INTRODUCTION

1.1. General

Integral abutment bridges have been used throughout the United States and several foreign countries. Traditional bridges are designed with expansion joints and other structural releases (Fig. 1.1a) that presumably allow the superstructure to expand and contract freely with changing temperatures. The integral abutment bridge (Fig. 1.1b) is less costly because expansion joints are eliminated in the bridge deck, which reduces the initial construction cost as well as continued maintenance costs. However, when expansion joints, roller supports, and other structural releases are eliminated, thermal forces are introduced into the bridge and must be accounted for in the design. The stresses produced in the abutment piling are the topic of this report.

Over half the state highway agencies have accepted the design of integral abutment bridges, but all have their own limitations on a safe length for such bridges [1–3]. For example, the Federal Highway Administration [4] recommends the following values as length limitations for integral abutments with continuous spans:

Steel	300 ft
Cast in place concrete	500 ft
Pre- or post-tensioned concrete	600 ft

The American Association of State Highway and Transportation Officials (AASHTO) does not address integral abutment bridges but does require that all bridge designs shall provide for thermal stresses or that means shall be provided for the thermal movements [5, Secs. 8.5.2, 9.5.1, and 10.11].

1.2. Objective

The objective of this research is to verify experimentally a design procedure for piles in integral abutment bridges.

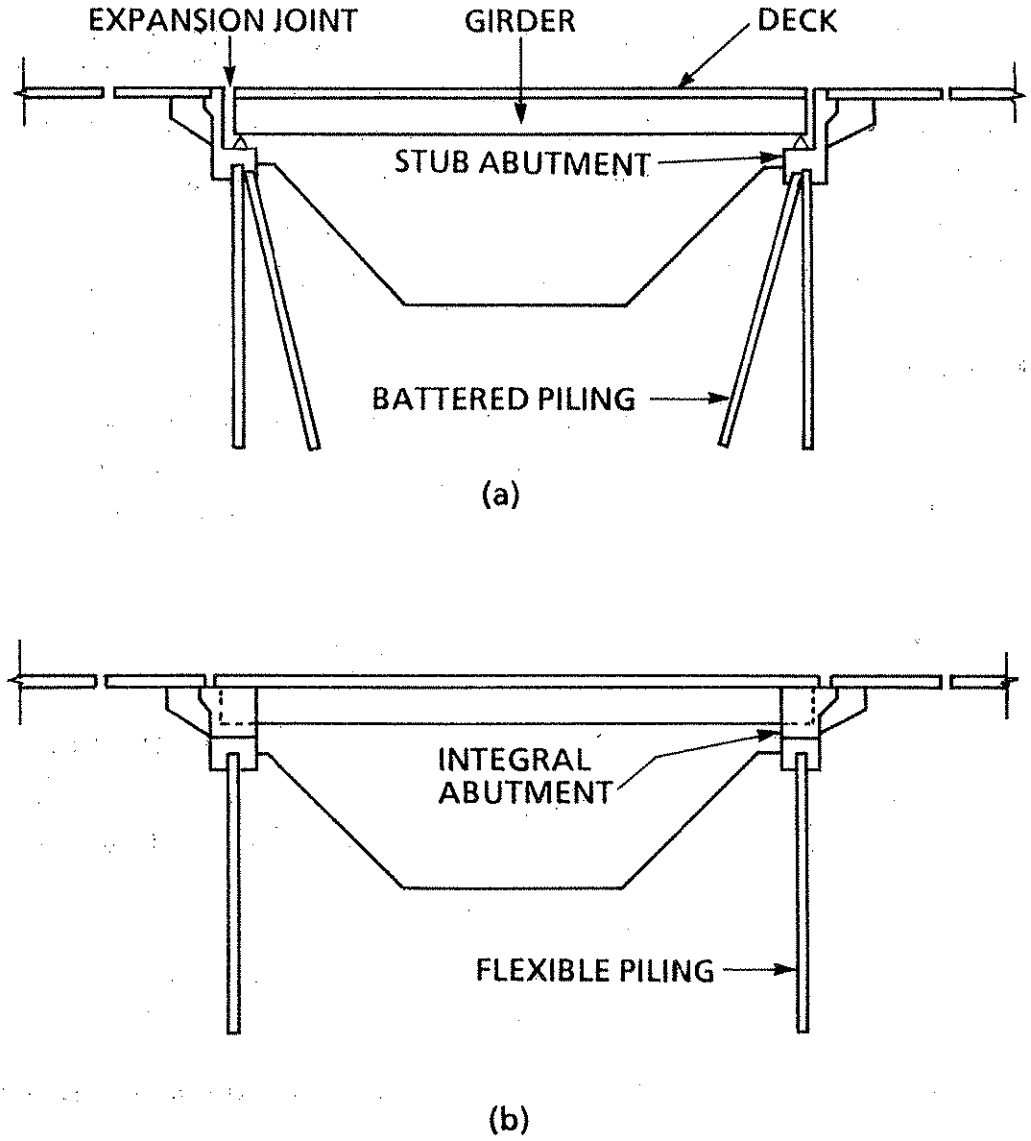

Fig. 1.1. Bridge abutment types: (a) bridge with expansion joints, (b) integral abutment bridge.

1.3. Project Overview

The project consisted of collecting experimental data (displacements, air and superstructure temperatures, and pile strains) for roughly two years and comparing them with analytical results from equations developed in previous studies [1,3,6–10].

Design recommendations are made for two types of bridges (precast concrete and steel). Factors considered in the design recommendations are the actual bridge temperatures, the effective coefficients of thermal expansion, and the strains in the abutment piling. A design example is presented.

1.4. Literature Review

1.4.1. Bridge Temperature and Expansion

Actual temperatures within a bridge superstructure differ from the ambient air temperature. Imbsen et al. [11] used empirical data (normal, daily minimum and maximum air temperatures) to obtain the minimum and maximum effective bridge temperatures. Emanuel and Hulsey [12] developed equations for the minimum and maximum ambient air temperatures and their corresponding solar flux (solar radiation). They used simple models based on computerized reductions of 20 years of weather data near Columbia, Missouri. Churchward and Sokal [13] correlated minimum and maximum ambient air temperatures and insolation (solar radiation) with the temperatures in the bridge cross section. On the basis of studies by previous authors, Reynolds and Emanuel [14] suggested methods to predict the superstructure temperature given the ambient air temperature. AASHTO [5, Sec. 3.16] states that "due consideration shall be given to the lag between air temperature and the interior temperature of massive concrete members or structures" and gives the following range of structure temperatures:

Metal Structures:	**Temp. Ranges**	
Moderate climate	0° to 120° F	
Cold climate	-30° to 120° F	
Concrete Structures:	**Temp. Rise**	**Temp. Fall**
Moderate climate	30° F	40° F
Cold climate	35° F	45° F

Temperature distributions through the depth of the superstructure have also been studied by several authors. Emanuel and Hulsey [12] and Prakash Rao [15] developed temperature distributions based on two-dimensional and one-dimensional heat flow models, respectively. A numerical solution was used to determine the distribution through the depth, and a finite element model was developed to determine the initial conditions and boundary conditions. Churchward and Sokal [13] collected temperature data through the depth of a concrete box-girder bridge for a three-year period. From these data, the authors developed equations relating the superstructure temperature to the ambient air temperature. Kennedy and Soliman [16] proposed a linear-uniform vertical temperature distribution based on theory and experiment.

Several papers [17–20] presented methods to estimate the thermal stresses in concrete and composite bridges. Soliman and Kennedy [17] and Hulsey and Emanuel [18] estimated thermal stresses by imposing compatibility conditions and solving strain equations at the interface of the concrete deck and steel beams. Radolli and Green [19] developed empirical design equations for thermal stresses in superstructures that are based on climatic data, for example, the ambient air temperature and solar radiation. The design equations can be used with a variety of superstructure geometries. Rahman and George [20] used a numerical approach to determine thermally induced stresses. They also presented a finite element model for a continuous span, skewed bridge.

1.4.2. Coefficient of Thermal Expansion

AASHTO [5] specifies the coefficient of thermal expansion for concrete as 0.000006 in./in./°F but all concrete does not exhibit the same coefficient of thermal expansion. It is a function of cement mix, aggregate types, mix proportions, temperature, and concrete age. The thermal expansion of concrete is the result of two processes occurring simultaneously [21]. The first is the normal thermal expansion common to all anhydrous solids (aggregates) and the second is the hydrothermal expansion or contraction caused by the movement of internal water in the capillary and gel pores of the concrete paste phase.

Since aggregates make up 80 to 85% of concrete, the thermal properties of the aggregates highly influence the coefficient of thermal expansion of a given concrete. Rhodes [21] reports values ranging from 3 to 6 μ in./in./°F for some limestones. The paste occupies 15 to 20% of concrete by volume and may exhibit an expansion coefficient ranging from 5 to 12 μ in./in./°F. Davis [22] found that the aggregate coefficient of expansion has the greatest effect

on the coefficient of expansion of the concrete. Callan [23] and Griffith [24] determined that the source and mineral composition (silica content) are the most influential factors that affect the thermal coefficient of expansion of aggregates.

Meyers [25] found that the coefficient of expansion of concrete increases to a maximum value when the moisture content is approximately 70% of saturation and decreases to a minimum value at 100% saturation. His test results also showed that the coefficient of thermal expansion of concrete will decrease slightly with age. Zuk [26] determined apparent coefficients of expansion for several types of bridges from experimental data. Emanuel and Hulsey [27] developed an effective means of predicting the thermal coefficient of expansion, which is based on the thermal characteristics of coarse and fine aggregates, relative humidity, and temperature:

$$\alpha_c = f_T(f_M f_A \beta_P \alpha_S + \beta_{FA}\alpha_{FA} + \beta_{CA}\alpha_{CA}) \tag{1.1}$$

in which f_T represents the correction factors for temperature alternations (1.0 for controlled environment and 0.86 for outside exposure). The correction factors for moisture and age are f_M and f_A, respectively, as given in Fig. 1.2. The coefficient of thermal expansion for the saturated condition, α_S, is 0.000006 in./in./°F. The coefficients of thermal expansion for the fine and coarse aggregates are α_{FA} and α_{CA}, respectively. (Typical values are given in [27]). The proportions by volume of the paste, fine aggregate, and coarse aggregate are β_P, β_{FA}, and β_{CA}, respectively.

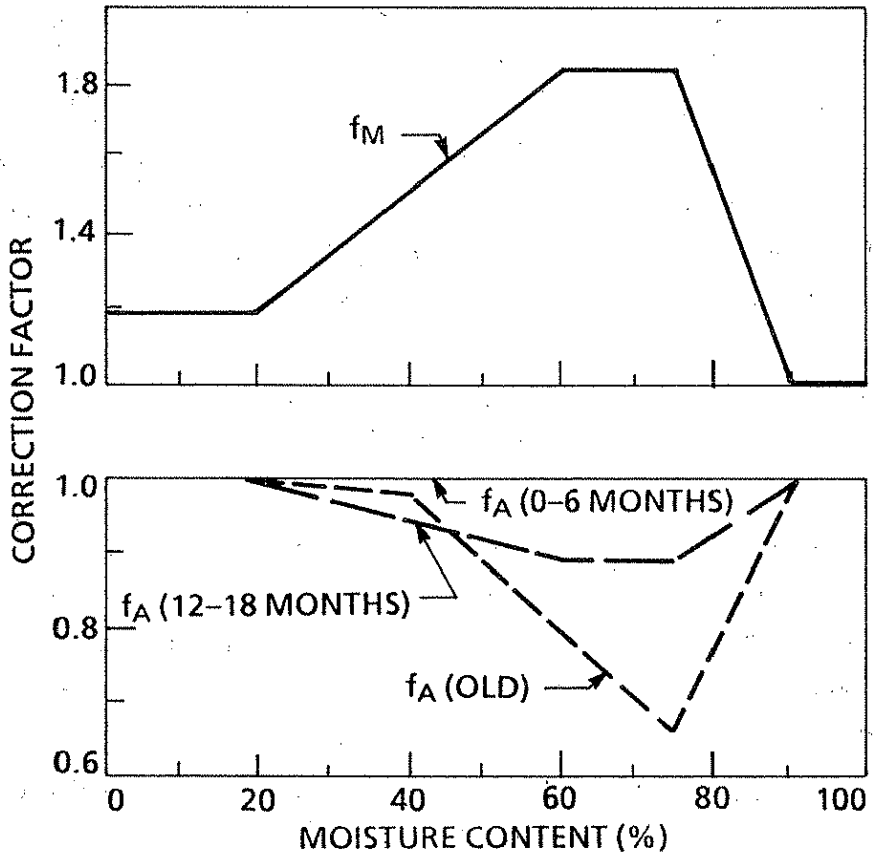

Fig. 1.2. Correction factors for moisture and age (adapted from Ref. [27]).

2. FIELD TESTS

2.1. Objective

A field testing program was conducted on two types of bridges in Iowa–a prestressed concrete beam and a steel girder–to collect bridge expansion data on deck and girder temperatures, air temperature, and pile strains. Coefficients of thermal expansion were determined from concrete cores taken from the two bridges.

2.2. Test Procedures

2.2.1. Test Sites

Field tests were performed on two bridges. The first is a prestressed concrete girder bridge, the Boone River Bridge, located in Webster City on county road R-33. Webster City is located in the central part of Iowa approximately 40 miles north of Ames. The second bridge, of steel girder construction, is the Maple River Bridge, located approximately one-half mile south of Danbury on county road L-37. Danbury is located approximately 40 miles east and 40 miles south of Sioux City.

Boone River Bridge

The Boone River Bridge is a concrete deck and prestressed girder bridge that spans 324.5 ft and is 40 ft wide. Figures 2.1, 2.2, and 2.3 show a plan, profile, and cross-sectional view, respectively, of the Boone River Bridge. The bridge is a continuous four-span bridge. Two of the piers are located approximately 80 ft from each abutment and the third pier is located in the center of the bridge. The prestressed girders are not integral with the piers but sit on neoprene pads approximately 1 in. thick. The rest of the structure is monolithically constructed. The skew angle of the bridge is 45°. The 7-1/2 in. deck is of reinforced concrete with a compressive strength of 3000 psi. The aggregate was primarily crushed limestone aggregate. The prestressed concrete girders are C80R type, as specified by the Iowa Department of Transportation (Iowa DOT), with a design strength of 5000 psi. The piles were driven in a predrilled hole approximately 9 ft deep with the strong axis parallel to the longitudinal direction of the structure and battered at a slope of 4:1 in the lateral direction only (Fig. 2.4).

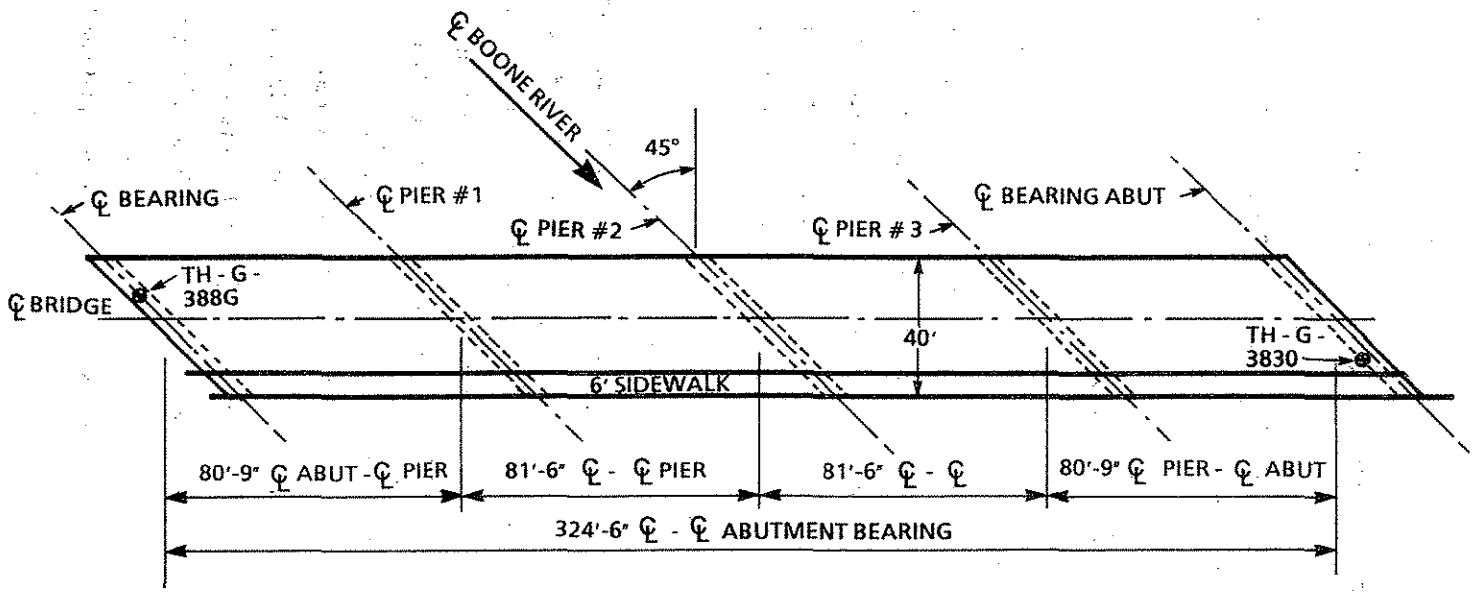

Fig. 2.1. Plan for the Boone River Bridge.

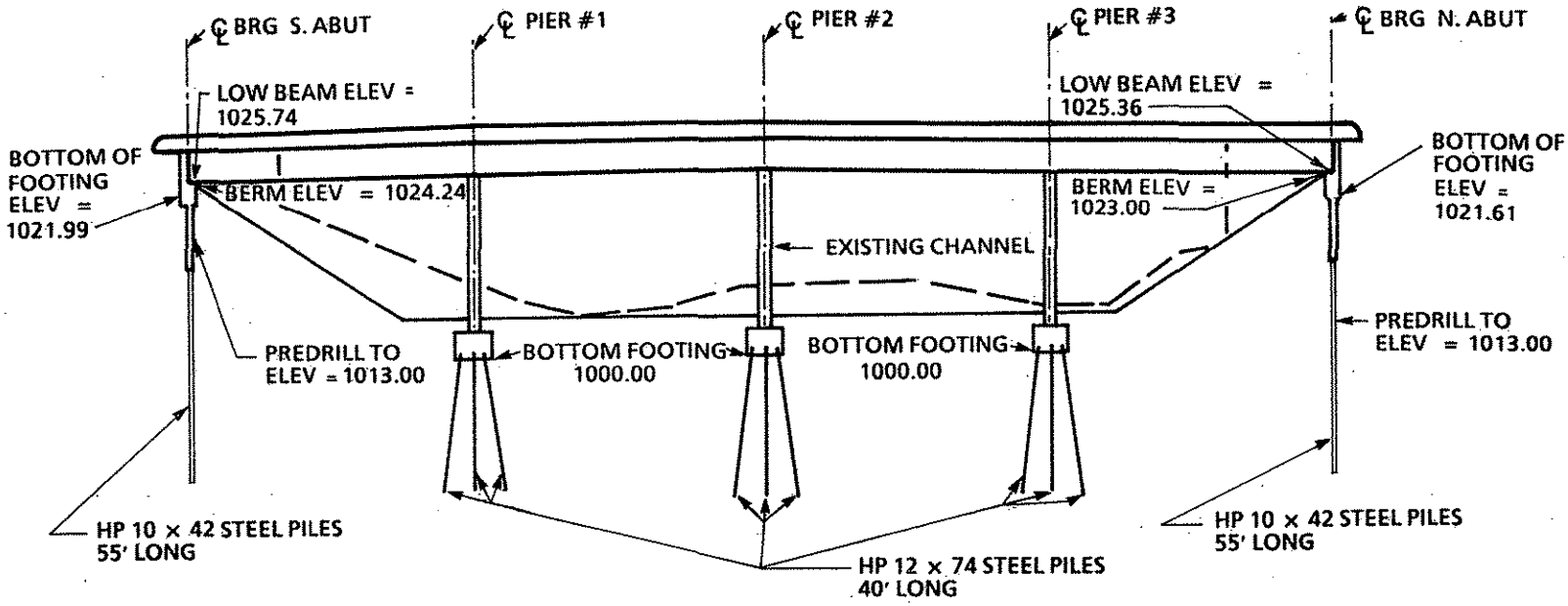

Fig. 2.2. Longitudinal section along center line of the Boone River Bridge.

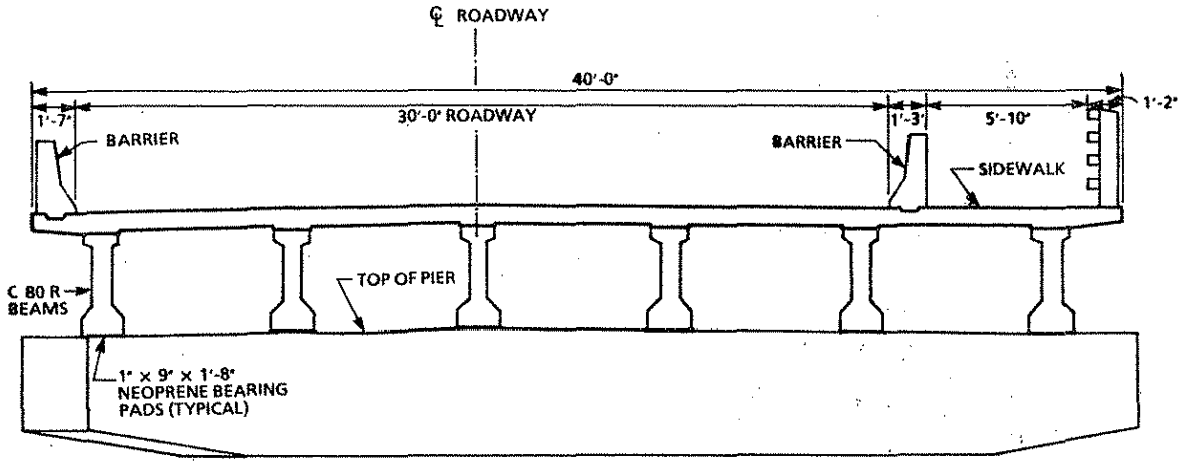

Fig. 2.3. Cross-sectional view of Boone River Bridge.

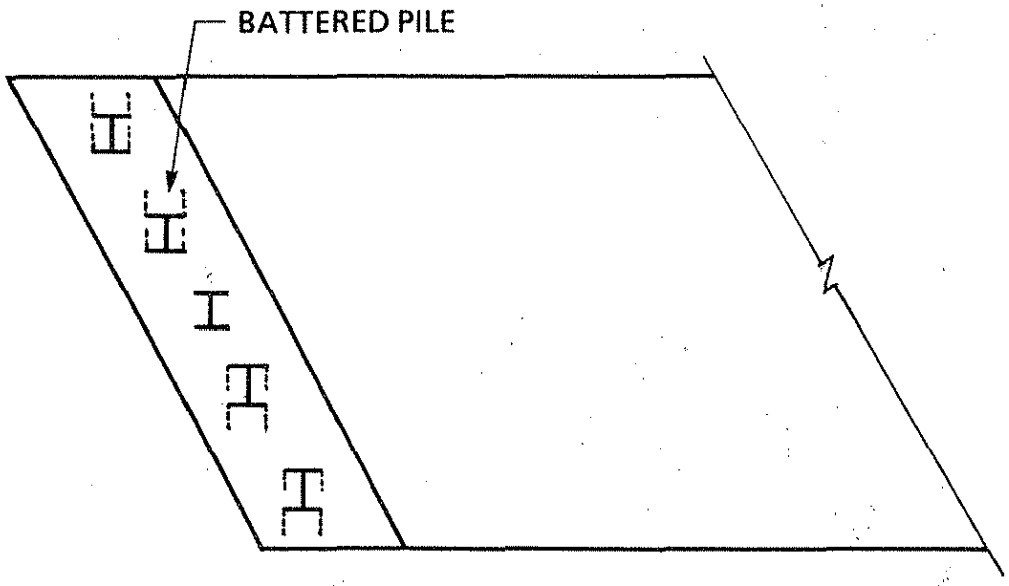

Fig. 2.4. Typical pile orientation (predominantly weak axis bending).

Maple River Bridge

The Maple River Bridge is a composite concrete deck and steel girder bridge, 320 ft long by 32 ft wide. Figures 2.5, 2.6, and 2.7 show a plan, profile, and cross-sectional view, respectively, of the Maple River Bridge. The bridge is a continuous three-span bridge with two piers located approximately 98 ft from each abutment. The Maple River Bridge has a skew angle of 30°. The abutments and girders were integrally cast with the deck to form a monolithic structure. The 8-1/2-in. deck is of reinforced concrete with a concrete compressive strength of 3500 psi. The coarse aggregate is gravel found in northwestern Iowa. The steel girders are welded plate girders approximately 49 in. deep and placed on bearing pads over the piers. The piles were driven in a predrilled hole approximately 12 ft deep with the strong axis parallel to the longitudinal direction of the bridge and battered at a slope of 3:1 in the lateral direction only (Fig. 2.4). Soil conditions are summarized in Appendix A.

2.2.2. Instrumentation

Typical instrumentation at each test site is described below. (Refer to Appendix A for additional information.)

Two linear variable differential transformers (LVDTs) were installed on the Maple River Bridge and one on the Boone River Bridge to monitor the longitudinal displacements. The LVDTs were placed at one end of each bridge under the overhang, in an electrical box. Each LVDT was clamped inside a spring with a known spring constant. The spring was attached to a wire, which was stretched across the entire length of the bridge. Nickel-iron wire was used because its coefficient of thermal expansion is extremely low (0.0000007 in./in./°F) over the temperature range encountered in the field. The wire had a diameter of 0.05 in. and was enclosed in a lubricated conduit to reduce frictional effects.

Surveying instruments were used to measure the bridge movement on a hot and cold day, as a check on the LVDT measurement.

Figure 2.8 shows a typical cross section and the locations of the thermocouples in the deck and girders. A copper-constantan type thermocouple wire was used. The thermocouple wires were placed in conduits to protect them from the environment. At the Boone River Bridge, holes were drilled in the precast girders and the thermocouple wires were placed inside the holes and sealed with grout. At the Maple River Bridge, the thermocouple wires

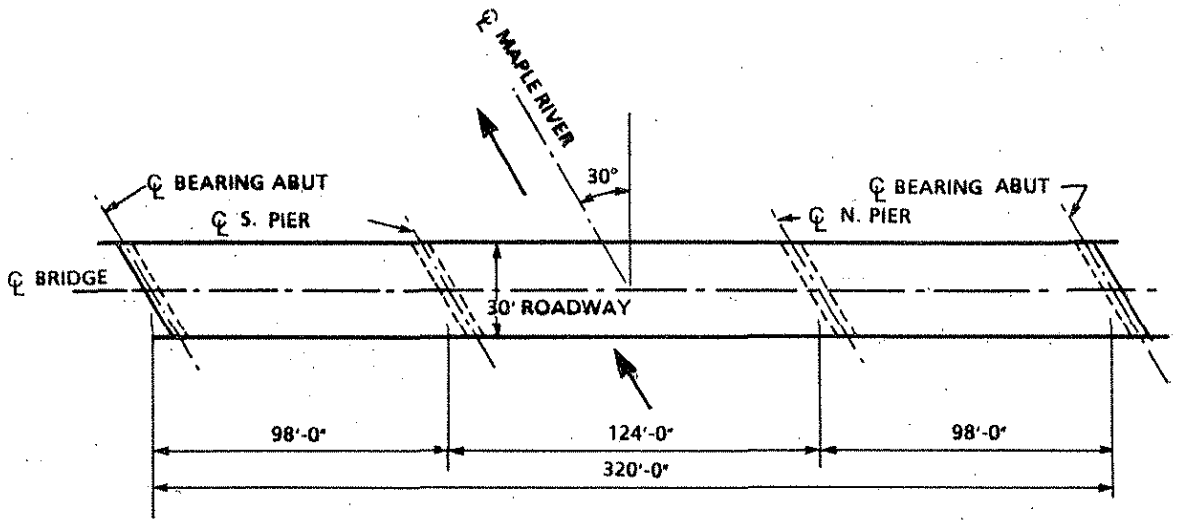

Fig. 2.5. Plan for the Maple River Bridge.

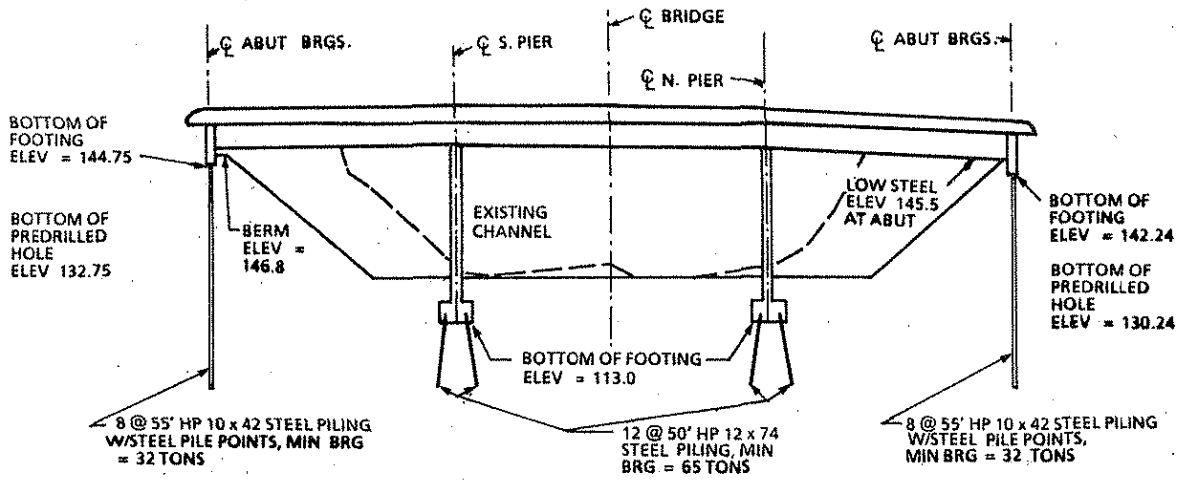

Fig. 2.6. Longitudinal section along center line of Maple River Bridge.

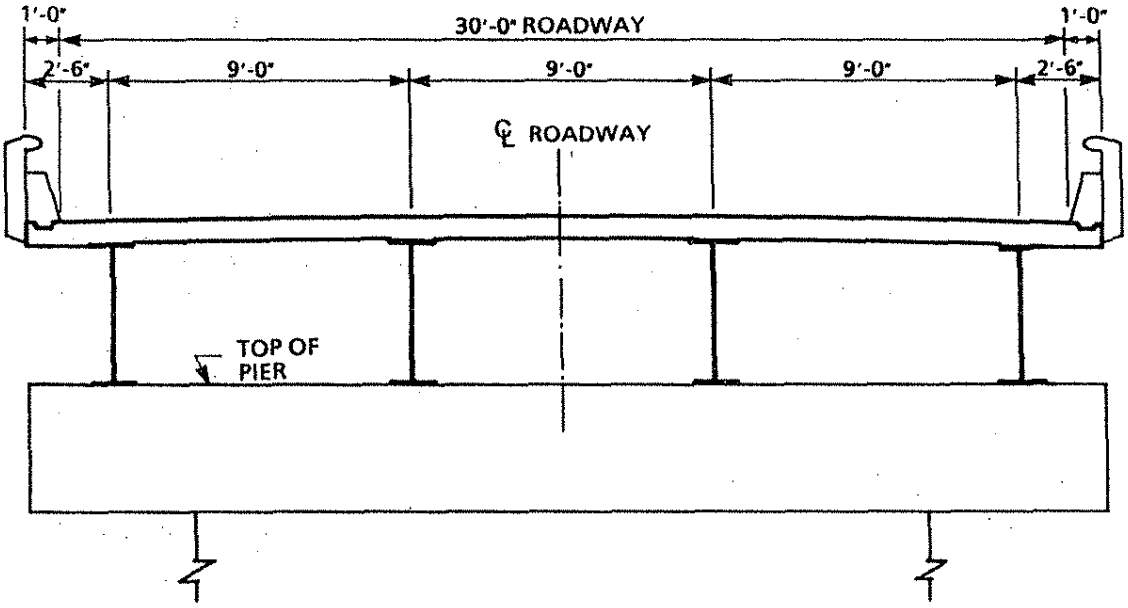

Fig. 2.7. Cross-sectional view of Maple River Bridge.

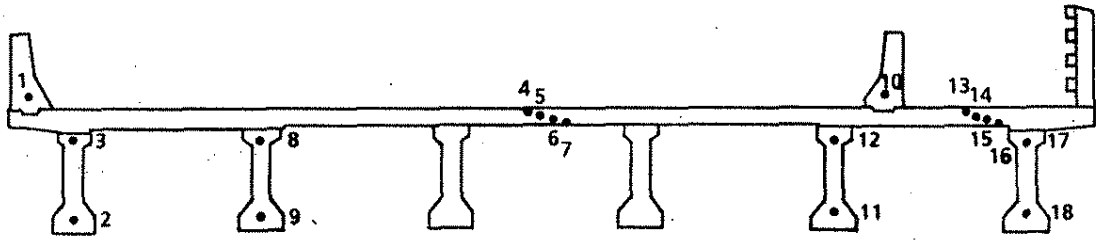

Fig. 2.8. Typical thermocouple locations.

were soldered to the exterior surface of the steel girders and enclosed in electrical junction boxes.

Four electrical resistance strain gages were placed on the second battered pile from the west end of each abutment. Only one pile at each bridge was instrumented with strain gages. Figure 2.9 shows the orientation and location of these gages. The strain gages were placed about 6 to 8 in. below the bottom of the abutment. Excavation was required at the pile-abutment interface, where approximately 3 ft of the pile was exposed for placement of the strain gages. The excavated area was left unfilled for the duration of the testing.

The control center was centrally located under one end of each bridge. All data were collected and stored in a Campbell Scientific computer, Micrologger 21X. The data were uploaded to cassette tapes about every 2 wks and transferred to floppy disks for permanent storage. The control centers were placed inside a security fence to protect against vandalism. Electrical hookups were provided by local power companies to meet the necessary electricity requirements. All instruments were enclosed in a junction box and the wires enclosed in conduits to protect against vandalism and environmental hazards.

2.3. Experimental Results

2.3.1. General

Data collection (LVDT and thermocouple readings) started on January 8, 1987, and ended on February 28, 1989, at both sites. The data collection for strain readings began on January 1, 1988, at the Boone River site and July 1, 1988, at the Maple River site and ended at both sites on February 28, 1989. Data were collected every 10 min. The six 10-min readings were averaged for an hour. The hourly averages for each device were stored in the memory of the Micrologger 21X. The zero hundred hour (0000 military time) on October 1, 1988, was selected as the reference day at the Boone River Bridge and September 6, 1988, as the reference day at the Maple River Bridge. These dates were selected because the air temperature was very close to the mean air temperature for the 26-mo period.

2.3.2. Air Temperature

Figures 2.10 and 2.11 show the actual air temperature at the two sites. At the Boone River Bridge the low temperature, -25° F, occurred on February 11, 1988, and the high, 103° F, on August 15, 1988. A low temperature of -21° F occurred on February 11, 1988, and the high,

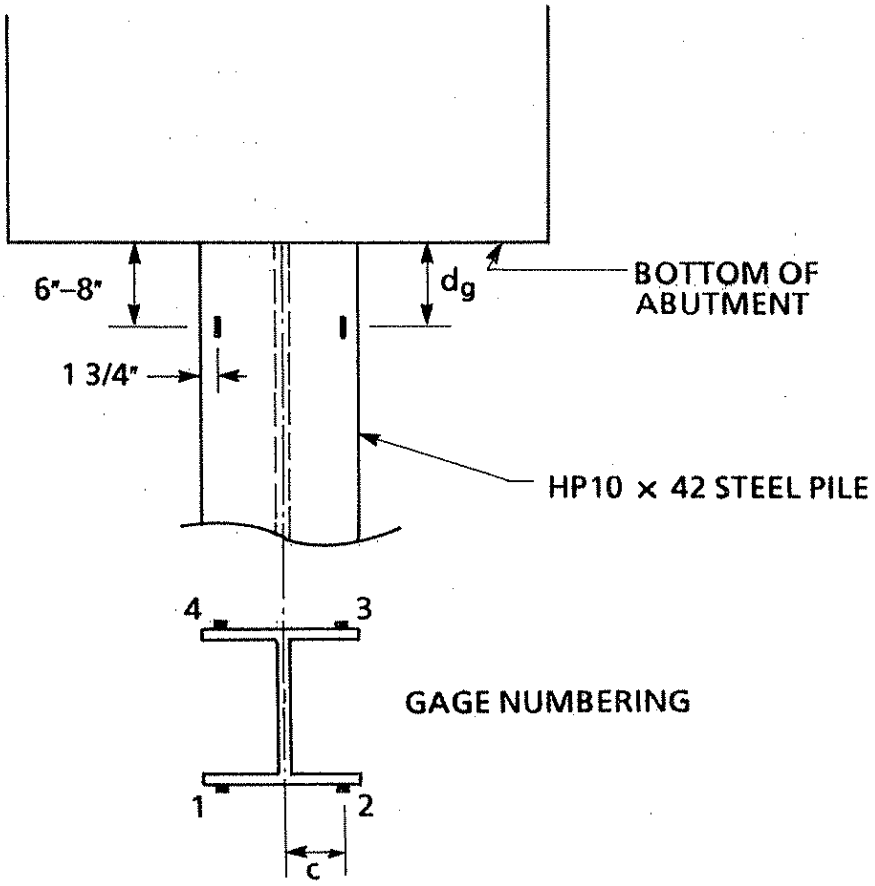

Fig. 2.9. Typical strain gage locations and numbering scheme.

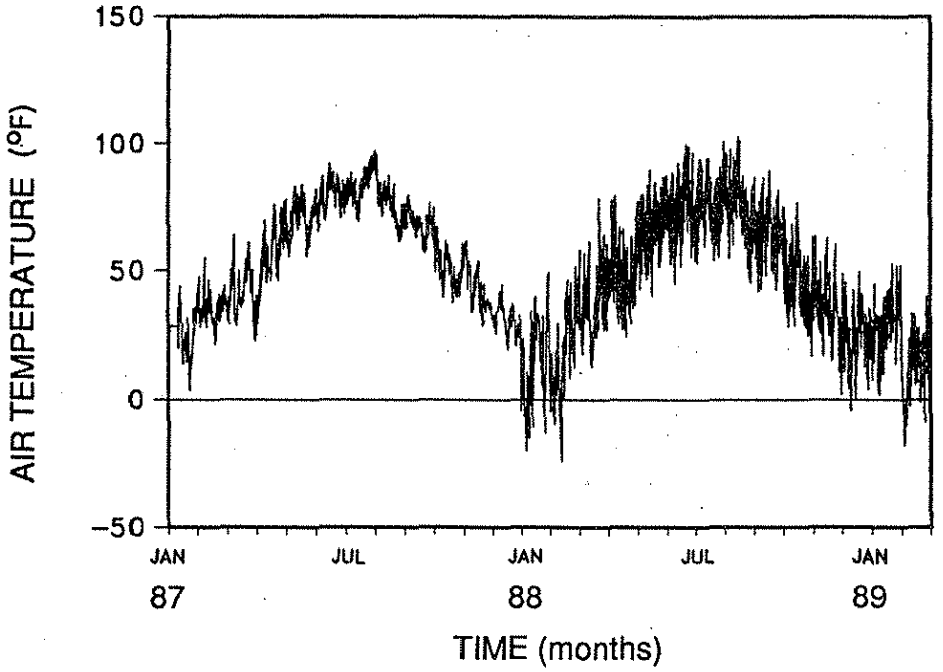

Fig. 2.10. Air temperature versus time for the Boone River Bridge from Jan. 1987 to Feb. 1989.

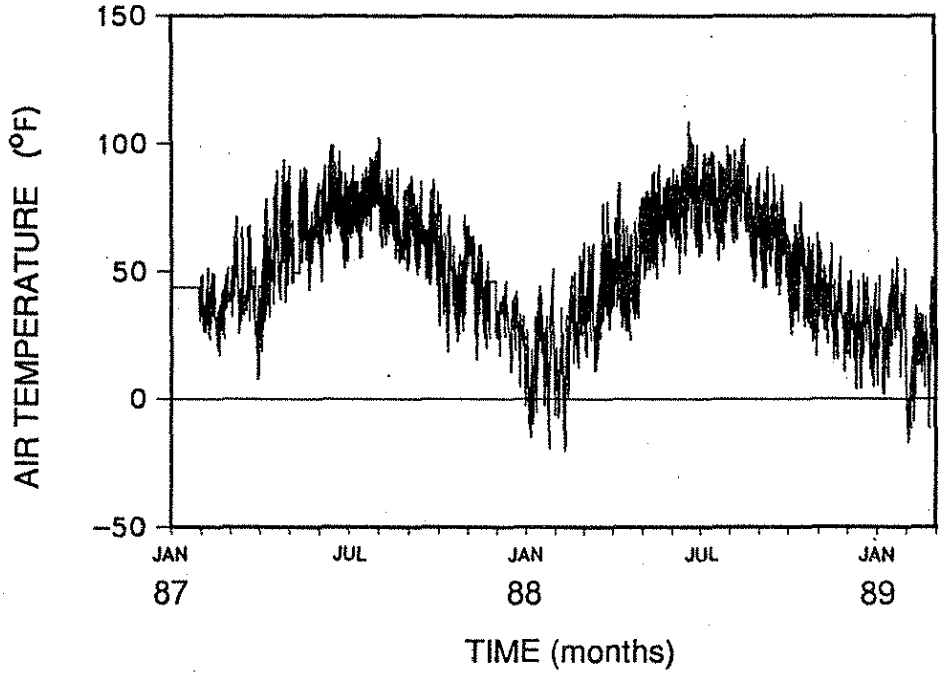

Fig. 2.11. Air temperature versus time for the Maple River Bridge from Jan. 1987 to Feb. 1989.

113° F, on June 20, 1988, at the Maple River Bridge. Both structures experienced roughly the same trend in air temperature over the 26-mo test period. The mean air temperature at both sites was about 55° F. The maximum air temperature range at the two bridges was 128° F and 134° F, respectively.

2.3.3. Bridge Temperatures

Bridge temperatures were recorded by the thermocouple wires that were placed in the deck and girders of the superstructure (Fig. 2.8). The hottest bridge temperature, which occurred in the deck near the upper surface, was approximately 120° F at the Boone River Bridge and 122° F at the Maple River Bridge. The coldest recorded bridge temperature of -16° F was fairly uniform throughout the superstructure of both bridges. Thus, the maximum temperature range for the deck at the Boone River Bridge was 136° F and 138° F at the Maple River Bridge. The maximum temperature range for the prestressed beams at the Boone River Bridge was 115° F and 117° F for the steel girders at the Maple River Bridge.

The temperature distribution through the depth of the deck and concrete girder is shown in Fig. 2.12 for the Boone River Bridge at the time of the hottest temperature. The distribution is similar for the Maple River Bridge. The distribution for the coldest bridge temperature is essentially uniform through the depth of the deck and girder system.

Temperatures were recorded across the width of the bridge also. The maximum temperature difference across the width was approximately 15° F at the time of the highest temperature.

2.3.4. Bridge Displacements

Figures 2.13 and 2.14 show the measured longitudinal displacements at the Boone River Bridge and the Maple River Bridge, respectively. The equation for the measured bridge displacement, Δ_b, is

$$\Delta_b = \Delta_s + \Delta_w + \alpha_w(\Delta T)L_w \tag{2.1}$$

where Δ_s is the spring displacement measured by the LVDT and equals P_s/k. (P_s is the force in the spring and k is the spring constant.) The thermal movements of the spring were considered negligible. The quantity Δ_w is the wire elongation caused by the longitudinal

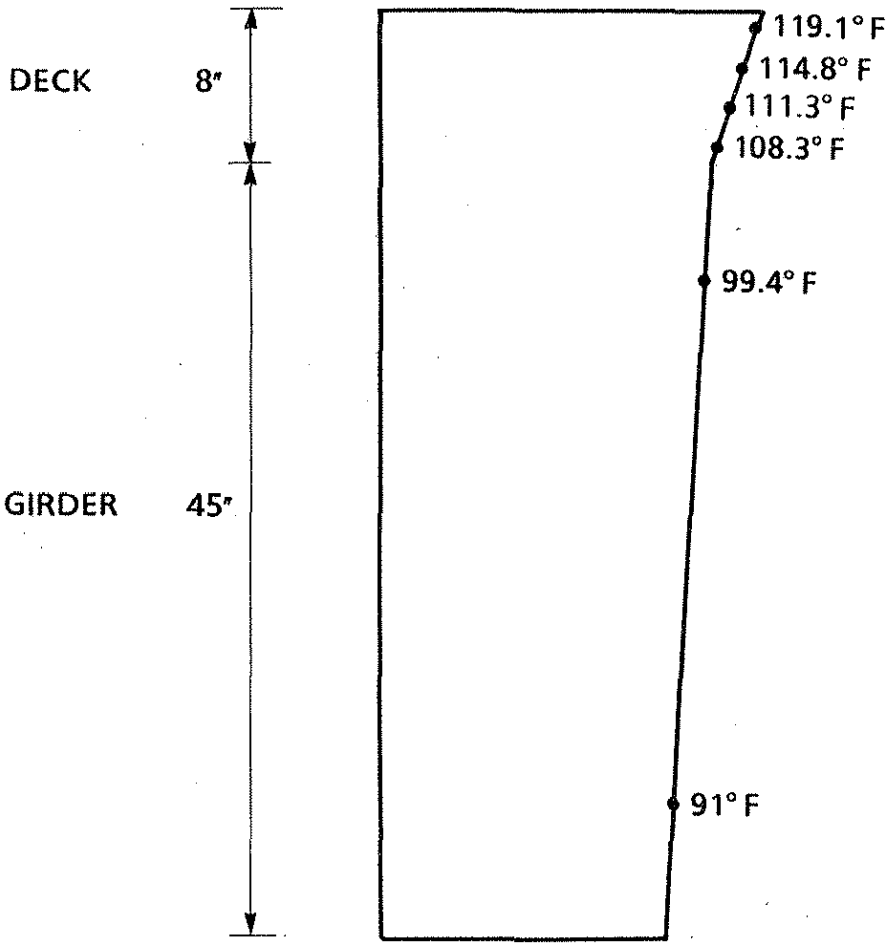

Fig. 2.12. Temperature distribution through the depth of the Boone River Bridge.

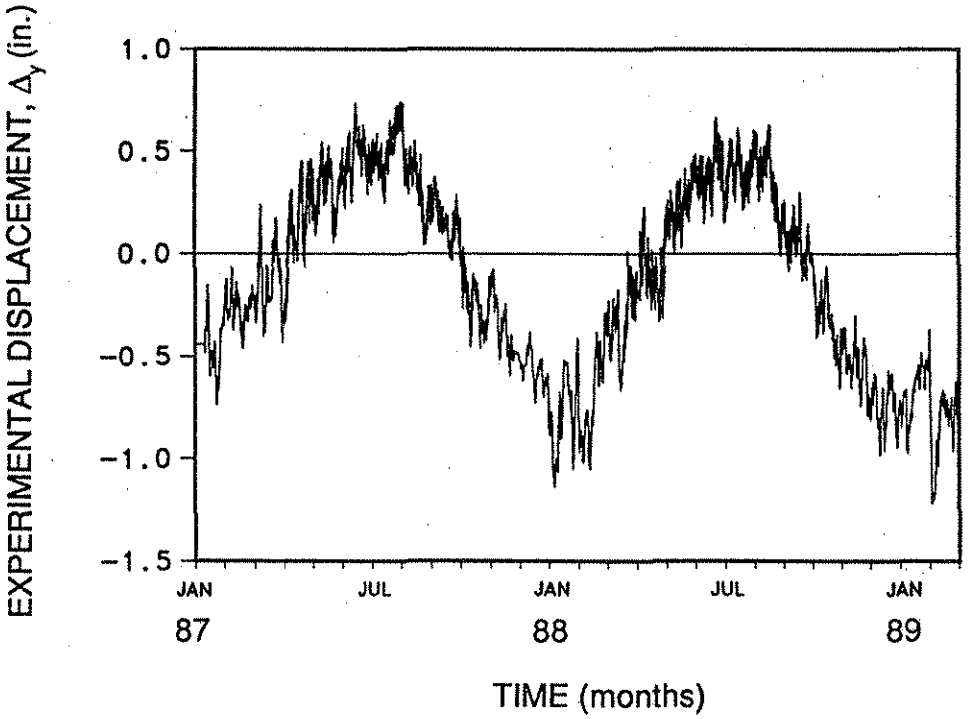

Fig. 2.13. Experimental longitudinal bridge displacement versus time for the Boone River Bridge from Jan. 1987 to Feb. 1989.

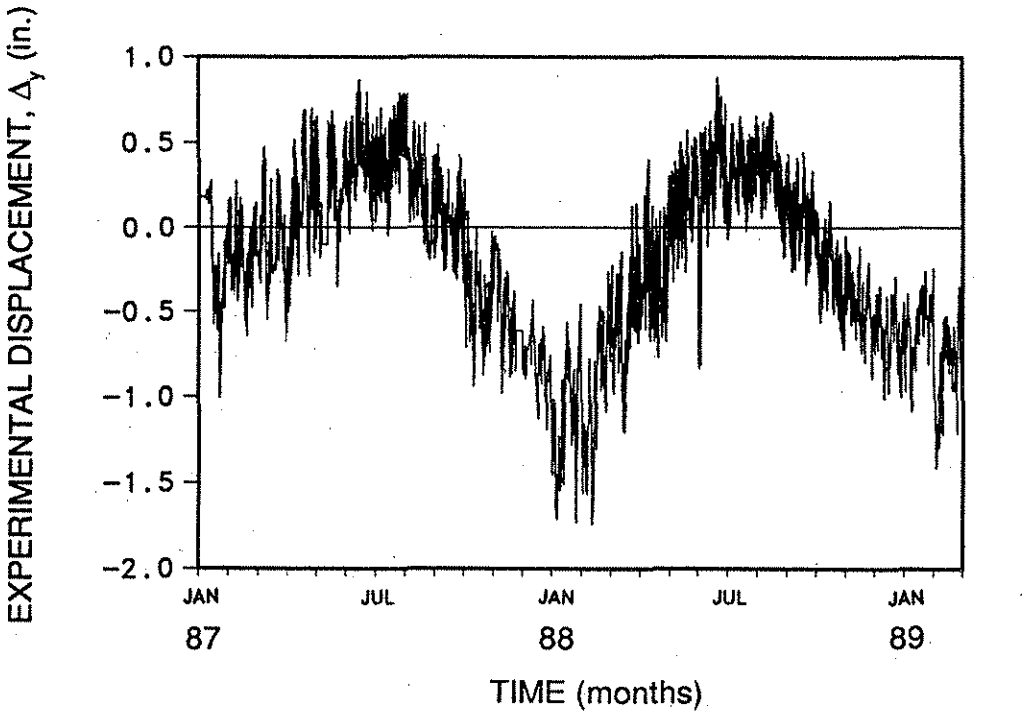

Fig. 2.14. Experimental longitudinal bridge displacement versus time for the Maple River Bridge from Jan. 1987 to Feb. 1989.

movement and equals P_sL/AE, where L is the length of wire, and A and E are the cross-sectional area and modulus of elasticity (approximately 21,000,000 psi) of the wire, respectively. The term $\alpha_w(\Delta T)L_w$ is the elongation of the wire due to temperature changes. A thermocouple was placed in the conduit to record the temperature of the wire. The Boone River Bridge had a total displacement range of approximately 2 in. and the Maple River Bridge had a total displacement range of approximately 2-1/2 in. Surveying instruments showed longitudinal displacement ranges of 1.8 in. and 1.9 in., respectively. (The surveying measurements were not made on the hottest and coldest days.)

There were pile bending strains about the strong axis (Sec. 2.3.5), which suggest that lateral displacements also occurred. Lateral displacements were not measured directly.

2.3.5. Pile Strains

Figures 2.15 and 2.16 show the pile strains caused by bending about the weak axis, ε_y, for the Boone River and Maple River bridges, respectively. Likewise, Figs. 2.17 and 2.18 show the pile strains caused by bending about the strong axis, ε_x, for the two bridges. The equation for the total measured strain, ε_m, is

$$\varepsilon_m = \varepsilon_a + \varepsilon_x + \varepsilon_y + \varepsilon_t \tag{2.2}$$

where ε_a is axial strain; ε_x and ε_y are the strains due to the bending about the x and y axis, respectively; and ε_t is the warping normal strain associated with torsional bending. At the Boone River site the four unknowns–ε_a, ε_x, ε_y, and ε_t–were isolated by solving four simultaneous equations involving the measured strain of the four gages (see Appendix A). Two components, ε_a, and ε_t, were relatively small in magnitude compared to the strains ε_x and ε_y and are not studied in detail here. [Note that the piles were oriented so that bending occurred predominantly about the weak (y) axis as the bridge expanded longitudinally; refer to Fig. 2.4.] At the Maple River site, the readings of one gage became erratic and only three gages were available in the calculations; hence, only three simultaneous equations were available. The torsional strain was assumed to be negligible since the torsional strain at the Boone River site was small.

Figures 2.15 through 2.18 show the experimental strain ranges due to temperature only. The strain ranges were approximately 700 to 900 μ in./in. for ε_y at the Boone River and Maple River bridges, respectively, and 200 to 300 μ in./in. for ε_x. Thermal strains will be

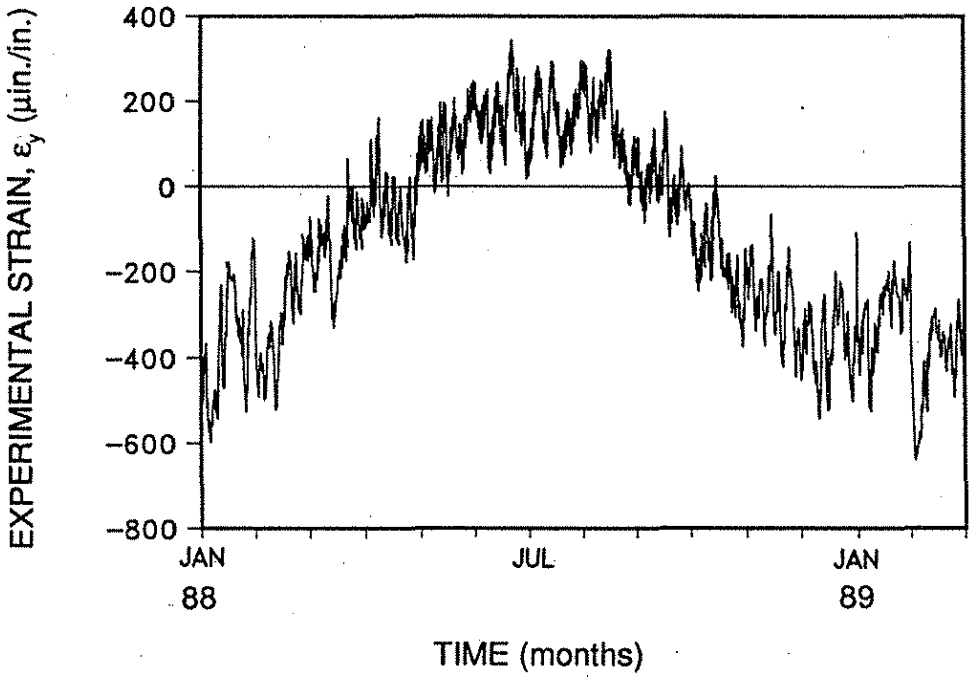

Fig. 2.15. Experimental weak axis strains versus time for the Boone River Bridge from Jan. 1988 to Feb. 1989.

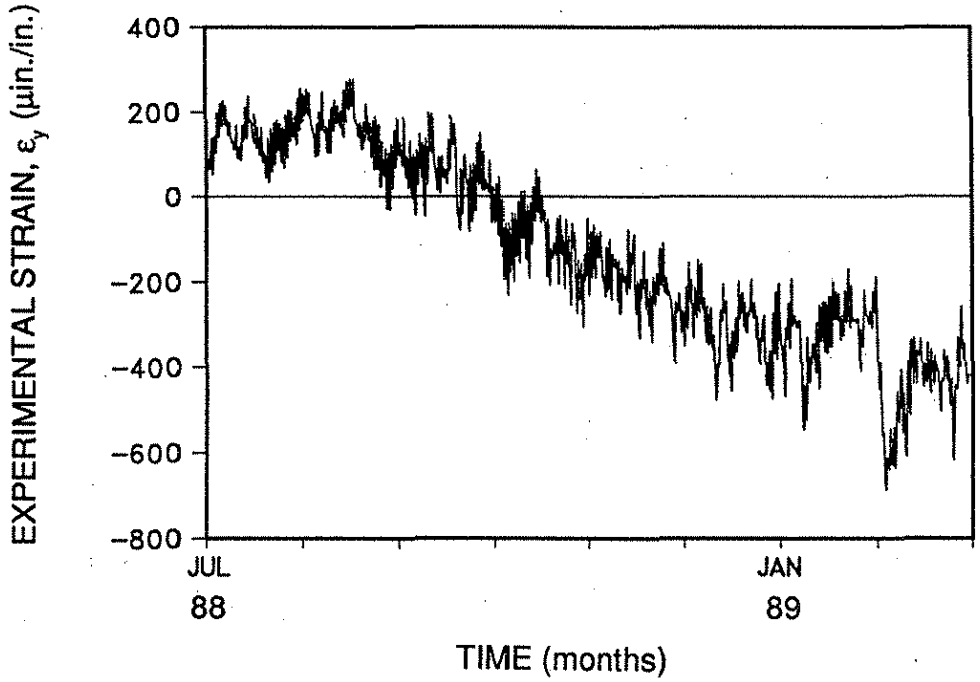

Fig. 2.16. Experimental weak axis strains versus time for the Maple River Bridge from July 1988 to Feb. 1989.

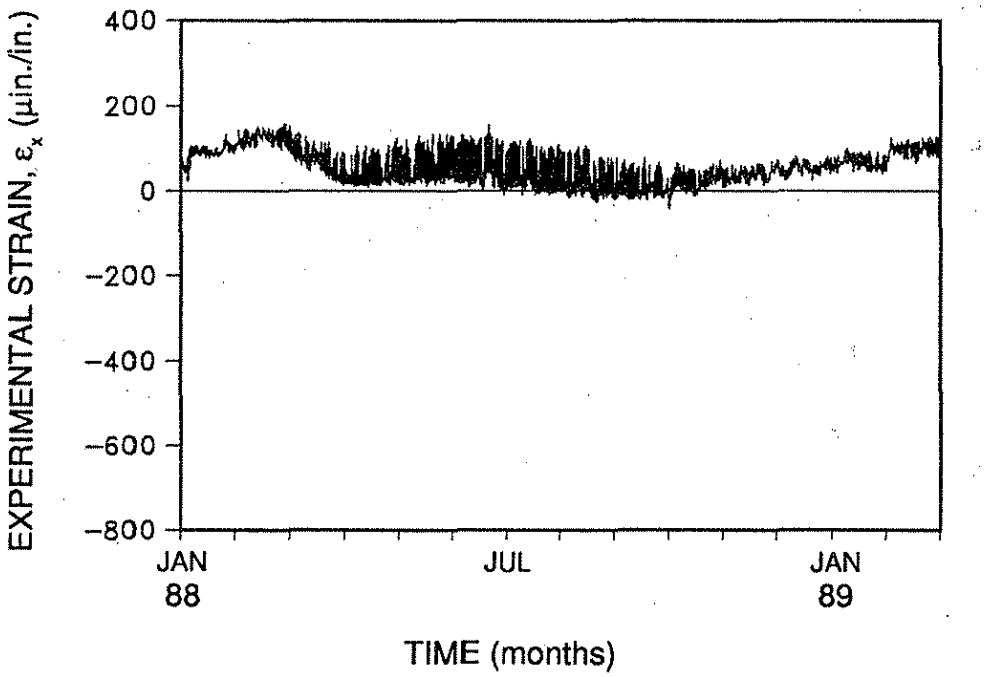

Fig. 2.17. Experimental strong axis strains versus time for the Boone River Bridge from Jan. 1988 to Feb. 1989.

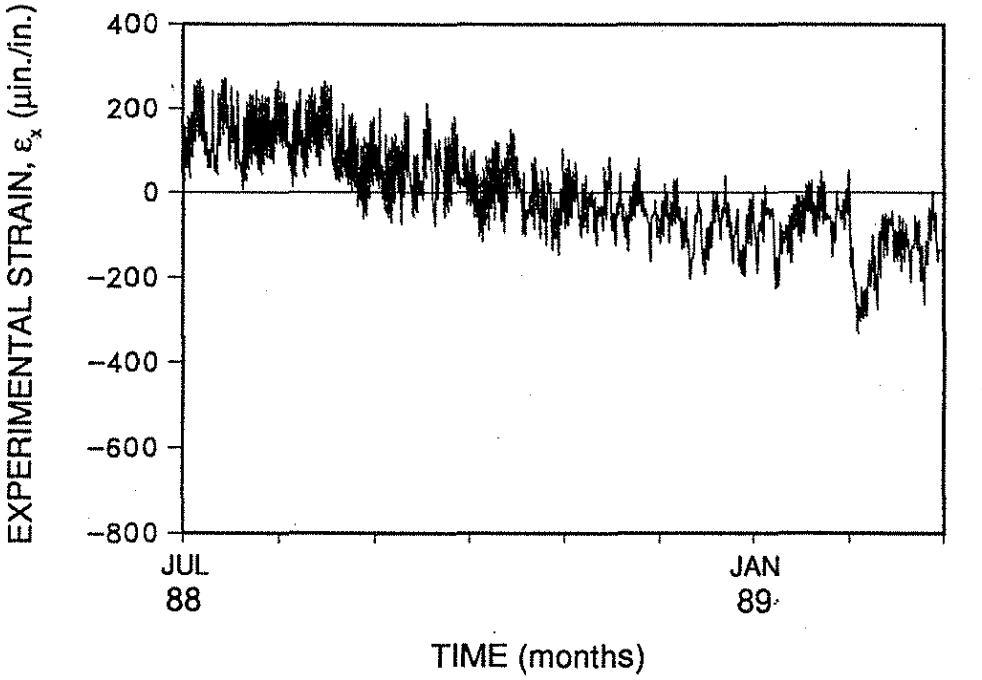

Fig. 2.18. Experimental strong axis strains versus time for the Maple River Bridge from July 1988 to Feb. 1989.

greater than this at the flange tips (beyond the strain gages) and just below the abutment (above the strain gages). Strains due to vertical and other loading are not included in the experimental values. The steel in the piles has a yield strain of approximately 1200 μ in./in. Most likely, yielding occurs at the flange tips up next to the abutment.

2.4. Coefficient of Thermal Expansion

2.4.1. Test Cores

Three core samples were obtained from the bridge abutments at each site. (Note: No cores were taken from the deck or girders.) The concrete from the Boone River site contained mostly crushed limestone aggregate, while that from the Maple River site consisted of a gravel aggregate mixture. The core samples were 4 in. in diameter and varied in length from 10 to 13 in. after trimming. Each sample was placed in one of three different moisture conditions (air dried, oven dried, and saturated) to determine the effective coefficient of thermal expansion.

2.4.2. Test Procedure

Tests were conducted in an environmental chamber capable of controlling both temperature and humidity. (Appendix B contains more information on the experimental setup and results.)

Each core sample was placed inside the chamber and subjected to changing temperatures (a heating and cooling cycle). The internal temperature and displacement were recorded at hourly intervals. Coefficients of thermal expansion versus time are illustrated in Appendix B.

2.4.3. Results and Recommendations

Table 2.1 summarizes the test results. Stabilized values occurred when there was little change in the coefficients of thermal expansion. The highest value of the coefficient of thermal expansion is exhibited by the air-dried cores. The saturated cores showed the lowest values. This trend is consistent with the literature [21–27]. The limestone aggregate concrete (Boone River Bridge) has a smaller coefficient of thermal expansion than does the gravel concrete (Maple River Bridge). This is also in agreement with the literature.

Emanuel and Hulsey [27] developed an empirical equation to predict the thermal coefficient of expansion (Eq. 1.1). Their equation was compared to the laboratory values for the air-dried conditions. The input of the material properties into Emanuel and Hulsey's equation were from the Iowa DOT D57 mix for structural concrete. The results in Table 2.1 agree well. Values for the saturated and oven-dried conditions were also checked and agreed favorably.

Based on the preceding results, the recommended coefficients of thermal expansion for the concrete in the abutments of the Boone River and Maple River bridges are shown in Table 2.1. The values are slightly biased toward the heating cycle since this is the highest expansion phase in the field. Before utilizing these values for the design of other bridges, the following conditions should be kept in mind:

- The design values are for mature concrete. New concrete may have a higher coefficient of expansion. The factor f_A in Fig. 1.2 can be used to correct for age effects. The authors recommend that the value of mature concrete be used.
- The coefficient depends heavily upon the coefficients of the aggregate (Sec. 1.4.2). Hence, other limestone aggregate concrete could have a significantly different coefficient than the Boone River Bridge.
- Girder and deck concrete should be evaluated for the coefficient of expansion.

Table 2.1. Effective coefficients of thermal expansion (μ in./in./°F).

	Boone River		Maple River	
	Heating	Cooling	Heating	Cooling
Air Dried	4.2	4.5	4.5	5.2
Oven Dried	3.0	3.1	4.5	4.3
Saturated	3.5	3.4	4.0	4.0
Ref. [27][a]	4.7		5.2	
Design	4.5		5.0	

[a] Values were calculated with mature concrete and crushed limestone aggregate (Boone River Bridge) and gravel aggregate (Maple River Bridge).

3. THERMAL EXPANSION MODEL

3.1. Objective

A method to predict the longitudinal thermal expansion and contraction of bridge structures is developed and compared to experimental values. A frame model is also presented to predict longitudinal displacements.

As stated in Sec. 2.3.5, measured pile strains, ε_x, confirm that lateral motions also occurred, although they were not measured directly. A model for predicting lateral displacements is illustrated in Ch. 4.

3.2. Axial Displacement Model

An idealized model of a bridge cross section is shown in Fig. 3.1. The model is divided into n segments, with the assumption that each segment has the following properties: uniform temperature, uniform coefficient of expansion or contraction, and uniform modulus of elasticity. Only axial extensions of the bridge were considered in the development of the axial displacement model. Abutment rotations are not included; in addition, the forces on the abutment caused by the passive and active earth pressures were neglected. In other words, the axial stiffness of the deck and girder system was assumed to be large enough to be unaffected by the pile restraint and the soil surrounding the abutments. Figure 3.2 shows the unrestrained longitudinal displacement, Δ_j, of each segment, j, and equals

$$\Delta_j = \alpha_j(\Delta T_j)L_j \tag{3.1}$$

where α_j is the coefficient of thermal expansion, ΔT_j is the internal temperature change, and L_j is the length of each segment. The total longitudinal displacement of the bridge is Δ_b.

The expansion and contraction of the structure induce thermal forces in each segment:

$$F_{hj} = (\Delta_j - \Delta_b)\frac{A_j E_j}{L_j} \tag{3.2}$$

where A_j is the cross-sectional area, and E_j is the modulus of elasticity. Equilibrium of the horizontal forces requires that the summation of F_{hj} equals zero or

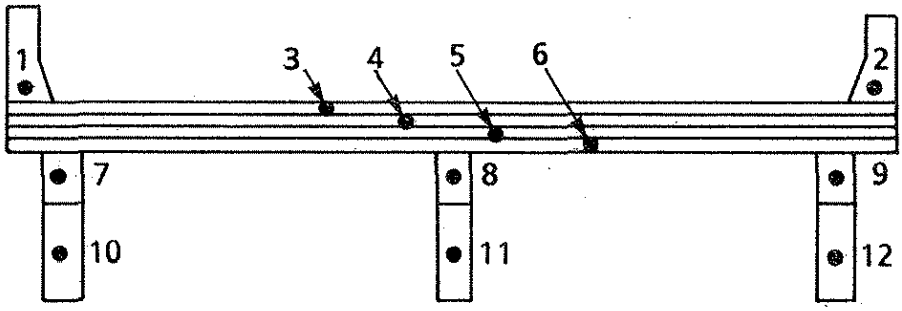

Fig. 3.1. Idealized bridge displacement model (axial only).

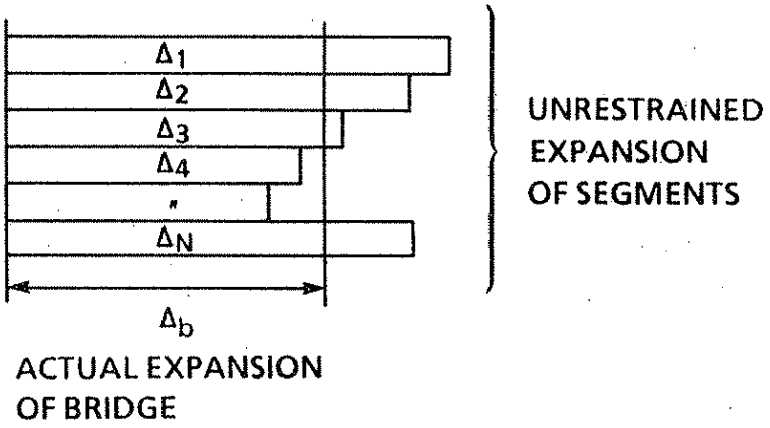

Fig. 3.2. Assumed displacement of each segment and overall bridge displacement.

$$\sum_{j=1}^{n} (\Delta_j - \Delta_b) \frac{A_j E_j}{L_j} = 0 \tag{3.3}$$

Assuming the length of all segments is equal to L and solving for Δ_b yields

$$\Delta_b = \frac{\sum_{j=1}^{n} \Delta_j A_j E_j}{\sum_{j=1}^{n} A_j E_j} \tag{3.4}$$

Substituting Eq. (3.1) into Eq. (3.4) results in the following equation for the longitudinal bridge displacement:

$$\Delta_b = \frac{\sum_{j=1}^{n} \alpha_j (\Delta T_j) A_j E_j}{\sum_{j=1}^{n} A_j E_j} L \tag{3.5}$$

The Boone River Bridge was subdivided into 16 segments corresponding to the thermocouple locations shown in Fig. 2.8. For example, the deck had eight segments, the guardrails had one segment each, and the beams had two segments (the upper thermocouple had approximately one-third of the beam cross-sectional area and the lower thermocouple had about two-thirds of the area). The temperature changes in all the segments were taken as the actual temperatures recorded by the corresponding thermocouples. The coefficient of thermal expansion of concrete was taken as 0.0000045 in./in./°F for the Boone River plot and 0.000005 in./in./°F for the Maple River plot (Table 2.1). (Remember that Table 2.1 values are for concrete in the abutment.) The same coefficient of thermal expansion was used for the deck and girders. The modulus of elasticity was 3,122,000 psi for the deck and 4,030,500 psi for the prestressed girders, which corresponds to 57,000 times the square root of the compressive strengths reported in Ch. 2. The Maple River Bridge is similar, except the girders are steel (α of 0.0000065 in./in./°F and an E of 29,000,000 psi) and the modulus of elasticity for the deck was 3,372,100 psi.

Figures 3.3 and 3.4 show the longitudinal displacements versus time for the Boone River and Maple River Bridges, respectively, from Eq. (3.5). The displacements shown in Figs. 3.3 and 3.4 (Boone River and Maple River Bridges, respectively) show the same trend in

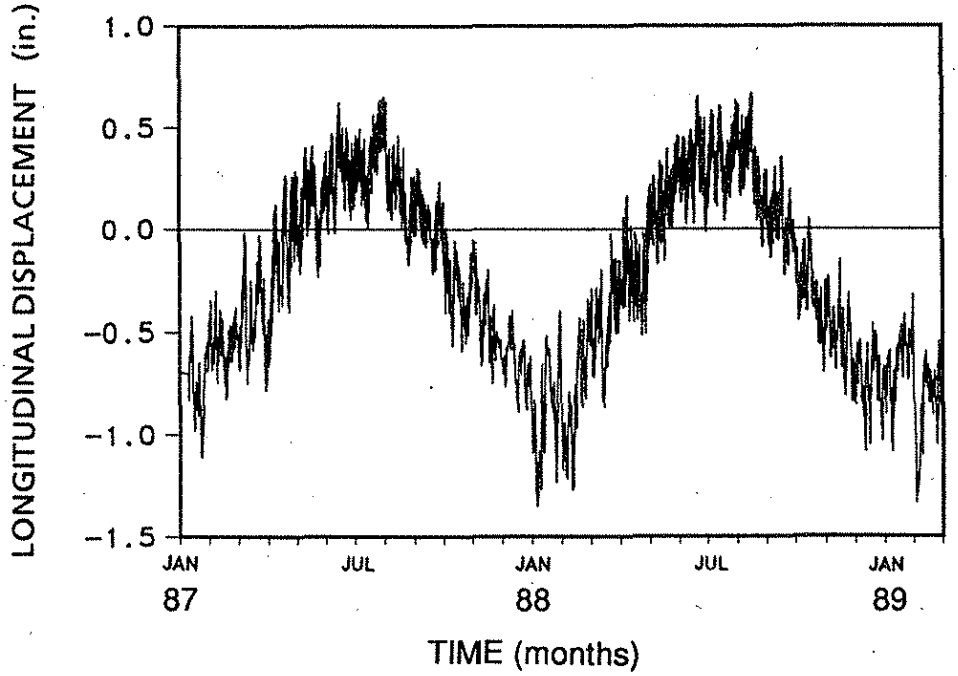

Fig. 3.3. Longitudinal displacements versus time for the Boone River Bridge from Jan. 1987 to Feb. 1989. [Eq. (3.5) and $\alpha = 0.0000045$ in./in./°F for concrete.]

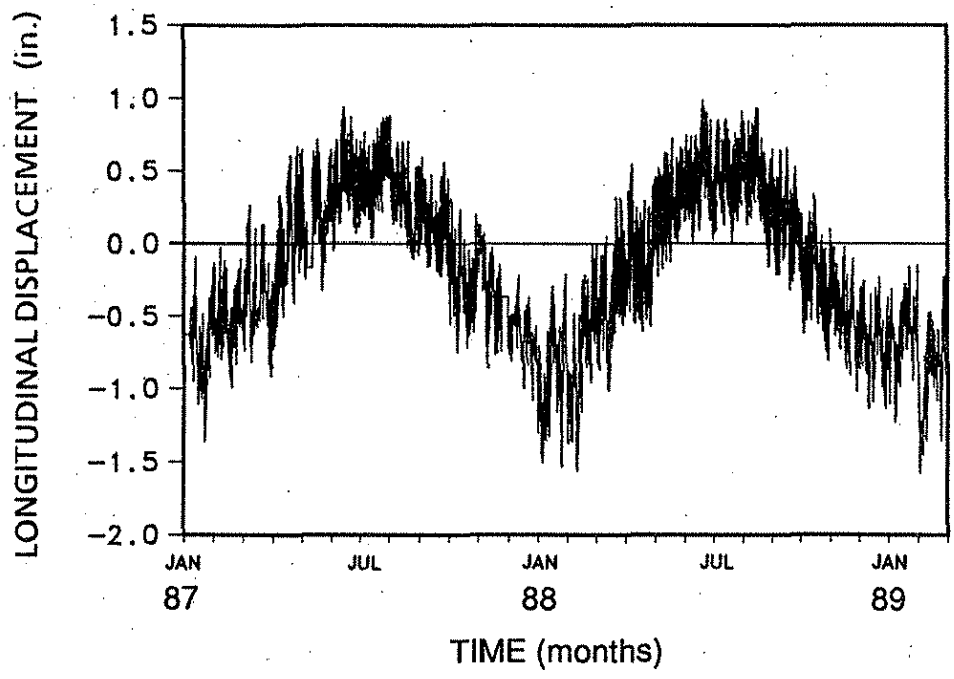

Fig. 3.4. Longitudinal displacements versus time for the Maple River Bridge from Jan. 1987 to Feb. 1989. [Eq. (3.5) and $\alpha = 0.000005$ in./in./°F for concrete.]

displacements over the 26-mo test period as do the experimental displacements shown in Figs. 2.13 and 2.14 (Boone River and Maple River bridges, respectively).

Since the coefficient of thermal expansion of concrete is quite variable, a range of values was studied. The bounding values used were 0.000003 in./in./°F to 0.0000045 in./in./°F for the Boone River Bridge and 0.000004 in./in./°F to 0.0000052 in./in./°F for the Maple River Bridge. These values represent the maximum and minimum stabilized values shown in Table 2.1. Figures 3.5 and 3.6 compare the experimentally measured displacements to the displacements calculated in Eq. (3.5). The maximum displacement ranges from Eq. (3.5) are shown in the two figures for the maximum range of bridge temperatures. The displacement range is the total movement due to bridge expansion and contraction. The axial model (Eq. 3.5) with the bounding coefficients of thermal expansion bounds the experimental displacements.

3.3. Longitudinal Frame Model

A two-dimensional frame model was developed to include the flexural stiffness of the piles and the axial and flexural stiffnesses of the deck and girders in the prediction of the longitudinal movement of each bridge. The passive and active earth forces were neglected because the corresponding displacements were small relative to the bridge movement. Only one-half of each structure was modeled because of symmetry. Figure 3.7 shows an elevation view of the two-dimensional frame model of the Maple River Bridge. This bridge is illustrated because of its composite construction.

The pile length, L_{My}, shown in Fig. 3.7 is the equivalent cantilevered length discussed in Sec. 4.3 and presented in Appendix C. Other member lengths are shown in Fig. 2.5. Nodal locations for the deck and girders were selected at the center of gravity of the respective elements. A node was placed at the location of the LVDT (bridge displacement, Δ_b) so that a direct comparison could be made with experimental displacements. Another node was similarly placed at the strain gage location. At the plane of symmetry, the nodal displacements were constrained against rotation and horizontal displacement. Rigid members were used to connect the deck and girder elements to simulate full composite action. At the pier, the steel girder and pier elements were allowed to rotate independently but the

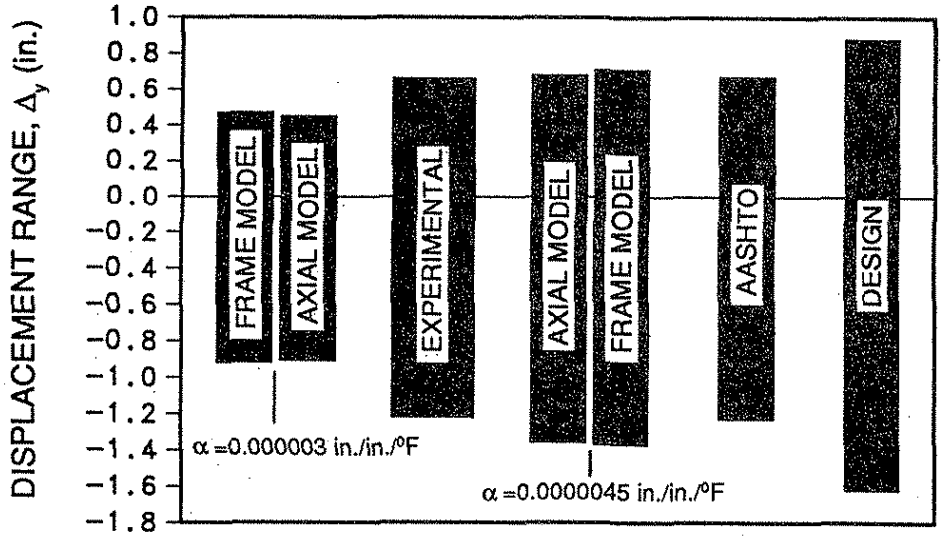

Fig. 3.5. Experimental and analytical longitudinal displacements for the Boone River Bridge.

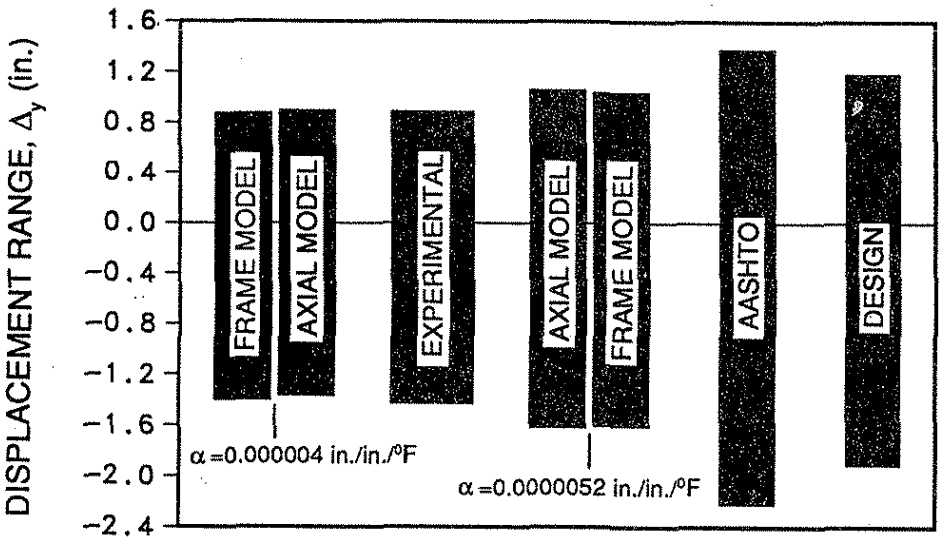

Fig. 3.6. Experimental and analytical longitudinal displacements for the Maple River Bridge.

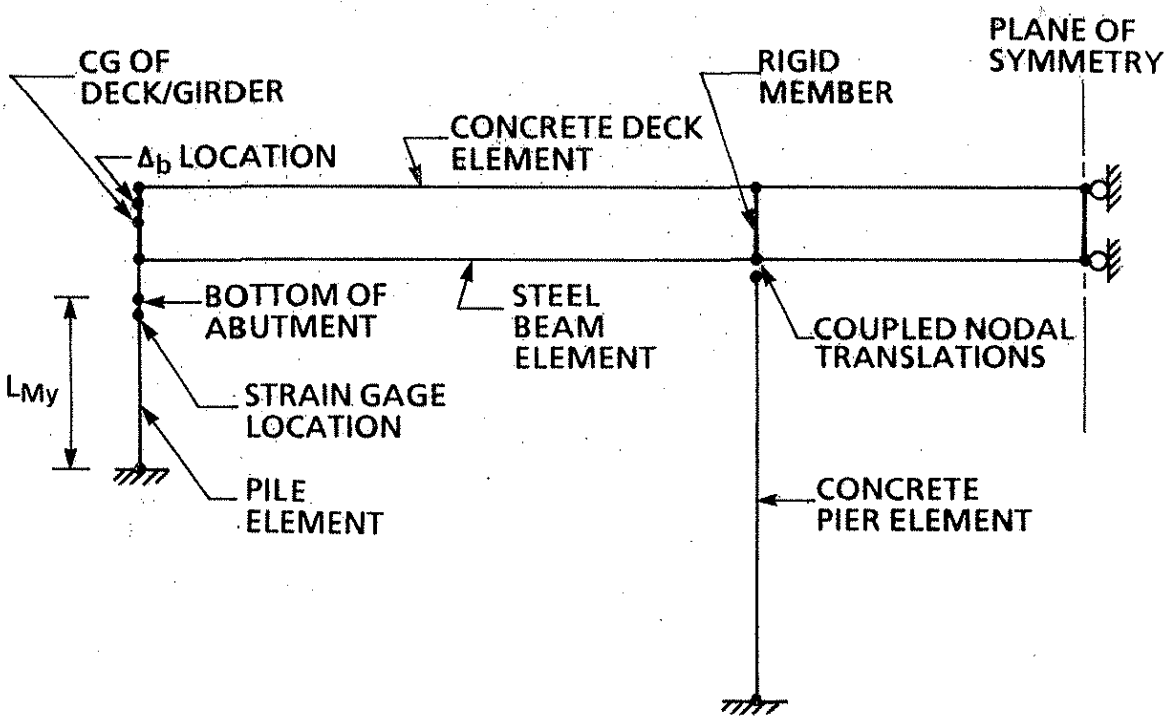

Fig. 3.7. Longitudinal frame model of Maple River Bridge.

horizontal and vertical displacements were coupled to move together. The Boone River Bridge frame model was similar to the Maple River model except for two things: (1) at the plane of symmetry, a rigid vertical support was provided to model the center pier (Figs. 2.1 and 2.2) and (2) at the intermediate pier, only the vertical displacement was coupled.

The linear temperature distribution shown in Fig. 2.9 was assumed to act on the deck and girder system of the frame model. Only three temperatures were used in the frame model, specifically, the temperatures at the thermocouples nearest the top of the deck, the deck and girder interface, and the bottom of the girder. The coefficients of thermal expansion were the bounding values used in Sec. 3.2. Figures 3.5 and 3.6 show the frame model's longitudinal displacements, which are approximately equal to the axial model's displacements; therefore, the axial model is satisfactory for predicting thermal longitudinal displacements.

3.4. Comparison with Experimental Displacements

The longitudinal displacement ranges for the axial and frame models (illustrated in Figs. 3.5 and 3.6) bound the experimental displacements. The displacements are dependent on the magnitude of the coefficient of thermal expansion of concrete.

3.5. AASHTO Longitudinal Displacements

The cold climate temperature ranges suggested by AASHTO [22, Sec. 3.16] are

Metal structures	T = 150° F
Concrete structures	T = 80° F

(The cold climate temperatures were used because the air temperature at both sites fell below -20° F). AASHTO suggests that the coefficient of thermal expansion for concrete be 0.000006 in./in./°F and for steel be 0.0000065 in./in./°F. Using Eq. (3.5) with one segment for the deck and one for the girders, we found the AASHTO longitudinal displacements are 1.9 in. and 3.6 in. (see Figs. 3.5 and 3.6) for the Boone River and Maple River bridges, respectively. The AASHTO displacement range is very close to the experimental displacement range for the Boone River Bridge. However, the AASHTO temperature range is significantly smaller than the range measured for this concrete bridge (Sec. 2.3.3) and the AASHTO coefficient of thermal expansion is significantly larger than experimental results (Table 2.1). It is a coincidence that the AASHTO displacements are approximately equal to the experimental values. At the

Maple River Bridge the AASHTO displacement range overestimates the experimental displacement shown in Fig. 3.6.

3.6. Recommendations

For purposes of calculating the longitudinal thermal expansion, a bridge should be divided into two segments: the deck and the girders. Either the axial model or the frame model can be used to predict the longitudinal displacements.

Design values of the coefficient of thermal expansion for the Boone River and Maple River bridges would be 0.0000045 and 0.000005 in./in./°F, respectively, both significantly below the AASHTO recommendation. In general, the value should be experimentally determined or predicted by some other means such as Eq. (1.1).

For design purposes, one would select an air temperature range larger than that recorded at the two sites over a two-year period only (Sec. 2.3.2). Hence, for design purposes one would select bridge temperature ranges higher than those measured in Sec. 2.3.3. In addition, concrete and steel bridge temperatures are not significantly different. The following values are recommended.

	Temperature Range
Concrete Deck	150° F
Concrete and Steel Girders	140° F

The longitudinal displacement ranges, using the above recommended values and Eq. (3.5), are shown in Figs. 3.5 and 3.6 for the Boone River and Maple River Bridges, respectively. The recommended design longitudinal displacements are 2.5 in. for the Boone River Bridge (versus 2 in. measured) and 3.1 in. (versus 2-1/2 in. measured) for the Maple River Bridge. The recommended coefficient of thermal expansion and temperature ranges give reasonable results for design purposes.

4. PILE STRAINS

4.1. Objective and Scope

The objective of this chapter is to verify a means for predicting the pile strains caused by the thermal expansion and contraction of integral abutment bridges. A comparison is made with the measured strains from Ch. 2.

4.2. Soil Characteristics

4.2.1. Pile and Soil Systems

Greimann et al. [1] used the Winkler soil model, shown in Fig. 4.1, to analyze soil-pile interaction. A finite element model and a design model were developed and compared. In both models, the springs represented the soil surrounding the pile. The lateral springs have an initial lateral stiffness, k_h, of the soil. The vertical springs have an initial vertical stiffness, k_v, of the soil and the point spring has an initial point stiffness, k_q, of the soil. In the finite element model the springs were assumed to behave nonlinearly. The design model, which is compared to the experimental results in this chapter, assumed linear springs.

4.2.2. Soil Properties

The only soil spring property needed for design purposes is the initial lateral stiffness, k_h. The equations and basic soil properties for determining the initial stiffness are listed in Table 4.1 (adapted from Ref. [1]). Typical soil properties for an HP 10x42 steel pile in clay and sand soils are listed in Table 4.2 [1]. The initial lateral stiffness, k_h, is assumed to vary linearly with depth for granular soils and to be constant for clay soils.

4.2.3. Initial Lateral Stiffness

Cross-sectional views of the south abutment of the Boone River Bridge and the north abutment of the Maple River Bridge are shown in Figs. 4.2a and 4.3a, respectively. Various soil layers, as determined by soil borings, are shown (refer to Appendix A also). The predrilled holes extended to 9 ft below the bottom of the abutment at the Boone River Bridge and to 12 ft

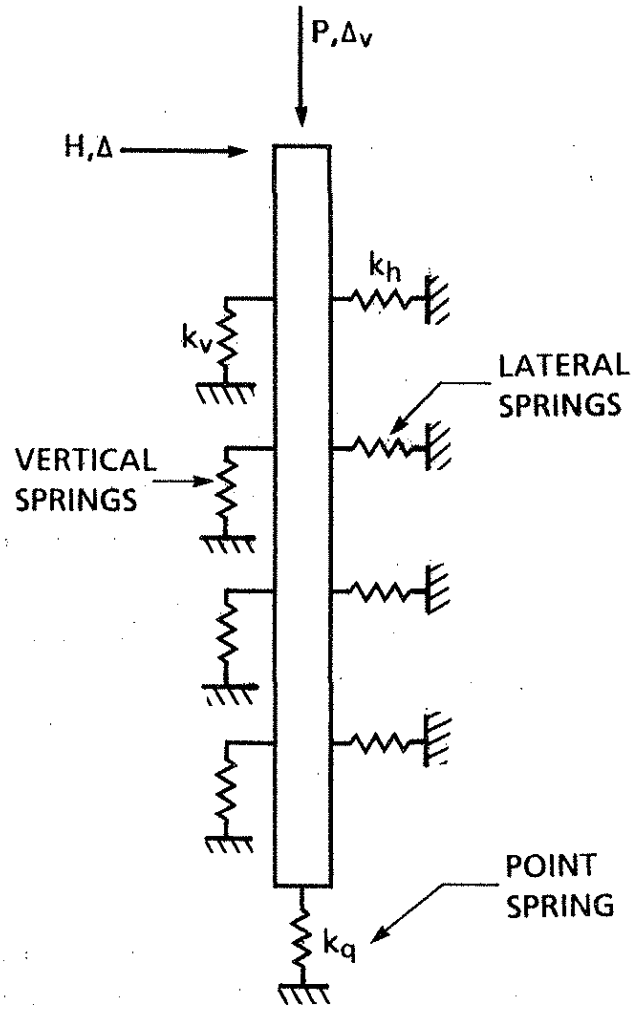

Fig. 4.1. Design model for soil-pile interaction (adapted from Ref. [1]).

Table 4.1. Initial stiffness, k_h, and basic soil properties.

Case	k_h	p_u (use lesser value)
Soft clay and stiff clay	$\frac{p_u}{y_{50}}$	$p_u = 9c_uB$ $p_u = \left[3 + \frac{\gamma}{c_u}x + \frac{0.5}{B}x\right]c_uB$
Very stiff clay	$\frac{p_u}{2y_{50}}$	$p_u = 9c_uB$ $p_u = \left[3 + \frac{\gamma}{c_u}x + \frac{2.0}{B}x\right]c_uB$
Sand	$\frac{J\gamma x}{1.35}$	$p_u = \gamma x[B(k_p - k_a) + xk_p tan\alpha tan\beta + xk_o tan\beta(tan\phi - tan\alpha)]$ $p_u = \gamma x\left(k_p^3 + 2k_p^2k_o tan\phi - k_a\right)B$

ε_{50} Axial strain at one-half peak stress difference from triaxial text; or use 0.02 for soft clay, 0.01 for stiff clay, or 0.005 for very stiff clay.
c_u Cohesion from an unconsolidated, undrained test
B Pile width
γ Effective unit soil weight
x Depth from soil surface
ϕ Angle of internal friction
k_p, k_a $= \tan^2(45° \pm \phi/2)$
k_o $= 1 - \sin\phi$
α $= \phi/2$ for dense or medium sand, $\phi/3$ for loose sand
β $= 45° + \phi/2$
J $= 200$ for loose sand, 600 for medium sand, 1500 for dense sand
y_{50} Displacement at one-half ultimate soil reaction: $2.5B\varepsilon_{50}$ for soft and stiff clay, $2.0B\varepsilon_{50}$ for very stiff clay.
p_u = ultimate soil resistance

Table 4.2. Soil properties for an HP 10x42 pile in clay and sand soils.

Clay	Soft	Stiff	Very Stiff
Blow count, N	3	15	40
Effective unit weight, γ(pcf)	50	60	65
Undrained cohesion, c_u (psf)	400	1,600	5,000
p_u (klf) (use lesser value)	3.0 or 1.0 + 0.24x	12 or 3.9 + 0.85x	37 or 12.5 + 10.1x
k_h (ksf) (use lesser value)	72 or 24 + 5.8x	580 or 190 + 41x	2,200 or 750 + 610x
Sand	**Loose**	**Medium**	**Dense**
Blow count, N	5	15	30
Effective unit weight, γ(pcf)	55	60	65
Angle of friction, ϕ	30°	35°	40°
p_u (klf)	$0.070x^2 + 0.12x$ for $x \leq 20$ 1.5x for $x > 20$	$0.15x^2 + 0.17x$ for $x \leq 18$ 2.9x for $x > 18$	$0.26x^2 + 0.24x$ for $x \leq 22$ 5.9x for $x > 22$
k_h (ksf)	8.0x	27x	72x

at the Maple River Bridge. The excavation for the strain gages exposed about 3 ft of the piling beneath the abutments.

Although soil borings were taken at the Boone River site, no quantitative soil investigations were performed. Shelby tube samples were collected at the Maple River site and an effective unit weight of 58 lb/ft^3 was determined at a depth of approximately 11 ft below the surface. Soil parameters, such as k_h, are very difficult to predict with any degree of certainty. The interaction of the loose sand in the predrilled hole with the surrounding material certainly complicated the prediction. In recognition of this, a range of parameters was considered. A range of stiffnesses versus depth are shown in Figs. 4.2b and 4.3b for the Boone River and the Maple River sites, respectively. At Boone River, the sand in the

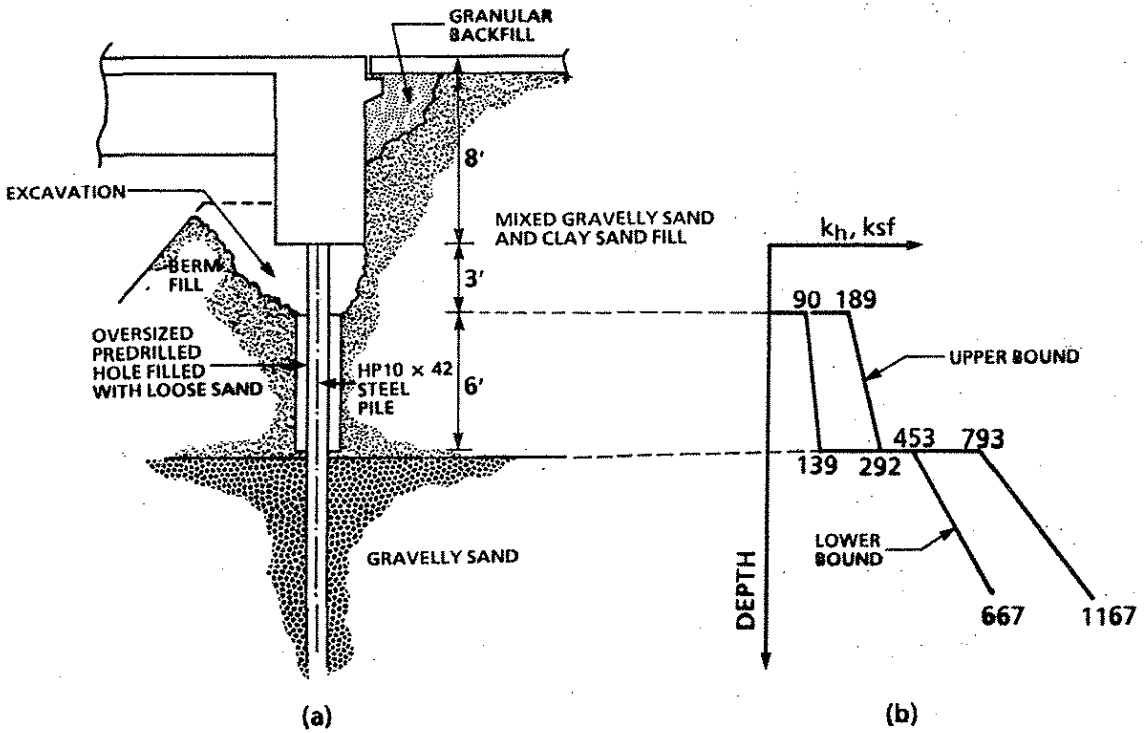

Fig. 4.2. Boone River Bridge: (a) cross section of abutment and pile, (b) initial stiffness versus depth.

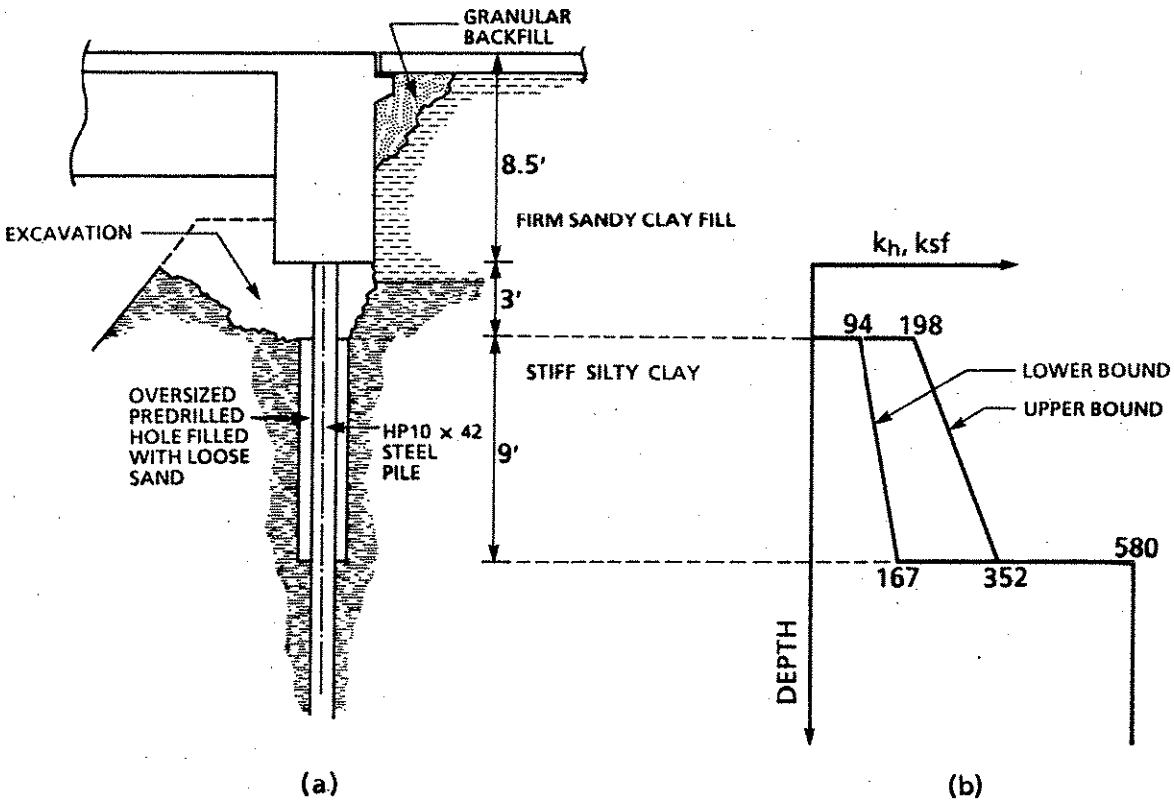

Fig. 4.3. Maple River Bridge: (a) cross section of abutment and pile, (b) initial stiffness versus depth.

predrilled hole and the surrounding in-situ soil was assumed to be bounded by loose sand and medium-loose sand. (The stiffness for medium-loose sand is the average of the stiffnesses for medium and loose sand in Table 4.2.) Below the predrilled hole, the in-situ soil was estimated to be between medium and dense sand. (The medium-dense stiffness is the average of the medium and dense sand in Table 4.2.) At the Maple River site, the sand in the predrilled hole acting with the surrounding soil was assumed to be bounded by loose sand and medium-loose sand. The in-situ soil below the predrilled hole was estimated to be stiff clay.

4.3. Pile Idealization

For purposes of analyses, a pile can be idealized as an equivalent cantilever [1]. Figure 4.4 illustrates the equivalent cantilevered system and the actual pile system. The length, ℓ_u, is the length from the pile head to the soil surface. The length, ℓ, in the actual system is the total length of the embedded pile below the soil surface. The equivalent length, ℓ_e, is the length of pile from the soil surface to the assumed fixed base of the equivalent system. The total length, L_e, of the equivalent system is the sum of the length of pile above the surface, ℓ_u, and the equivalent length, ℓ_e. The displacement, Δ (shown in Fig. 4.4), is the displacement of the abutment caused by thermal expansion and contraction of the superstructure.

To determine the equivalent length of a pile below the soil surface, a critical length parameter, ℓ_c, was first defined. For a pile embedded in soil, the critical length was the depth below which displacements and bending moments at the pile head have little effect. Piles longer than ℓ_c act as infinitely long piles. The critical length parameter for a uniform initial lateral stiffness, k_h, is [1]

$$\ell_c = 4\sqrt[4]{\frac{EI}{k_h}} \tag{4.1}$$

where E is the modulus of elasticity and I is the moment of inertia of the pile. For a pile in a nonuniform soil, an effective lateral stiffness, k_e, is determined. In Appendix C, a method is presented to calculate k_e.

Figure C.1 (Appendix C) shows three plots for determining the equivalent length, ℓ_e, for fixed-head piles based on three different equivalencies: (1) the horizontal stiffness of the

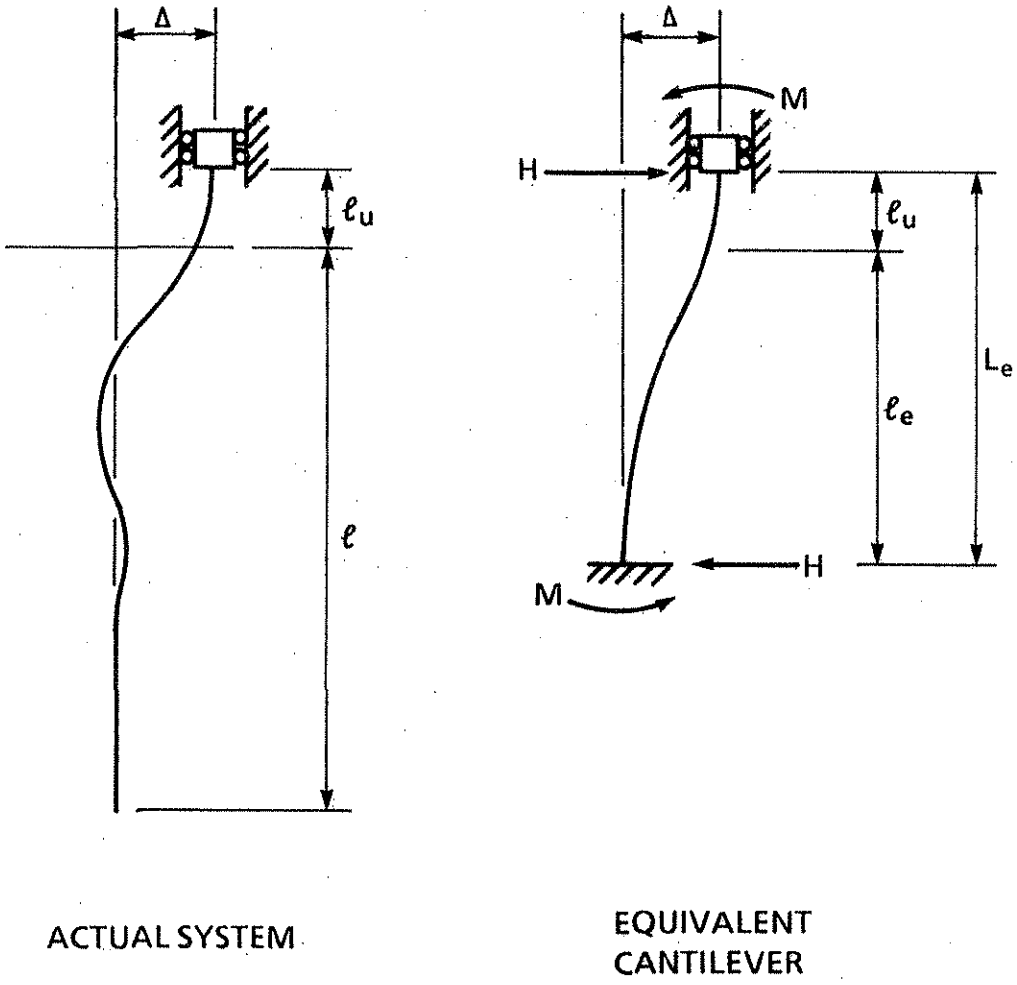

Fig. 4.4. Pile idealization as equivalent cantilever.

Table 4.3. Range of equivalent cantilevered lengths (in.).

Equivalent Lengths	Boone River	Maple River
L_{Hy}	107 to 94	106 to 94
L_{My}	115 to 100	114 to 98
L_{By}	155 to 148	186 to 187
L_{Hx}	132 to 116	133 to 115
L_{Mx}	142 to 125	144 to 122
L_{Bx}	177 to 165	203 to 187

soil-pile system, ℓ_{eh}, (2) the maximum moment in the pile, ℓ_{em}, and (3) the elastic buckling load of the pile, ℓ_{eb}. (Equivalent cantilevered lengths for pinned head piles are given in [1]). Only L_H, the total equivalent length for horizontal stiffness, and L_M, the equivalent cantilevered length for the moment, are used in this chapter. The length, L_B, is the total equivalent cantilevered length for elastic buckling. An example in Appendix C illustrates the procedure for determining the equivalent cantilevered lengths for the Boone River site.

Since the moment of inertia, I, is different about the x and y axes, there will be different equivalent lengths for strong and weak axes bending. (Note that the piles at both bridges are oriented to bend primarily about their weak axis as thermal movements occur. Strong axis bending corresponds to lateral bridge movement; see Fig. 2.4.) Table 4.3 lists the equivalent cantilevered lengths, L_H, L_M, and L_B, for both the strong and weak axes corresponding to the bounding soil stiffnesses shown in Figs. 4.2b and 4.3b. (The longer equivalent length is associated with the lower bounding stiffness).

4.4. Pile Strains due to Longitudinal Movement

4.4.1. Individual Pile Model

The displacements associated with the longitudinal thermal expansion and contraction of a bridge produced first-order elastic moments about the weak axis, y. Consider a fixed-head equivalent pile (Fig. 4.4) with a lateral displacement, Δ_y. Then the horizontal force, H_y, and the maximum moment, M_y (which occur at the top of the pile) are

$$H_y = \frac{12EI_y\Delta_y}{L_{Hy}^3} \tag{4.2}$$

$$M_y = \frac{6EI_y\Delta_y}{L_{My}^2} \tag{4.3}$$

The weak axes moment at the location of the strain gages is

$$M_{gy} = M_y - H_y d_g \tag{4.4}$$

where d_g was the depth from the pile head to the gage locations within the excavated area. (See Figs. 2.9, 4.2, and 4.3).

The normal stress, σ_y, at a distance c (Fig. 2.9) from the neutral axis is

$$\sigma_y = \frac{M_{gy}c}{I_y} \tag{4.5}$$

The strain can be related to the stress by Hooke's Law, ε equals σ/E. Combining Eqs. (4.2) through (4.5) with Hooke's Law gives the strain ε_y at a distance c from the neutral axis as

$$\varepsilon_y = \Delta_y c\left(\frac{6}{L_{My}^2} - \frac{12d_g}{L_{Hy}^3}\right) \tag{4.6}$$

The displacement, Δ_y, will be taken as one-half the total measured longitudinal elongation of the bridge, Δ_b (in Ch. 2).

$$\Delta_y = \frac{\Delta_b}{2} \tag{4.7}$$

This, of course, assumes the thermal expansion is symmetrical.

Figures 4.5 and 4.6 show the weak axis pile strains, ε_y, calculated by Eq. (4.6). The surrounding soil was assumed to be loose sand (Figs. 4.2b and 4.3b) for both plots. The results from Eq. (4.6) showed the same trends as the experimental strains presented in Ch. 2 (Figs. 2.14 and 2.15, the Boone River and Maple River Bridges, respectively), but the computed strains were slightly larger than the experimentally measured strains. Figures 4.7 and 4.8 for the Boone River and Maple River bridges, respectively, show the range of weak axis strains associated with two different, equivalent cantilevered lengths, one for each of the bounding k_h curves in Figs. 4.2b and 4.3b, respectively. The ranges in the corresponding experimental strains are also shown in those two figures.

4.4.2. Longitudinal Frame Model

As we developed Eq. (4.6), the pile head was assumed to be fixed against rotations (Fig. 4.9a) since the abutment and beams are much stiffer than the piles. Figure 4.9b shows the actual motion of the abutment, which includes an abutment rotation. The simplified frame model developed in Ch. 3 (Fig. 3.5) was used to verify that the rotations of the abutment were important in determining pile strains. However, abutment rotations were not important when determining bridge displacements.

The equivalent cantilevered length, L_{My}, used in the frame model (Sec. 3.3), was based upon a rigidly fixed pile head. The bending stiffness of the piles was much less than that of the girders and deck so that a fixed-head assumption was more appropriate here than a pinned head. The development of equivalent cantilevered lengths for elastically restrained pile heads was not deemed necessary.

Specified longitudinal displacements, namely one-half the measured displacement range shown in Fig. 2.13 and 2.14, were applied to the frame model at the symmetry plane (the center of the bridge).

The weak axis strains resulting from the longitudinal frame analysis are shown in Figs. 4.7 and 4.8 for the Boone River and Maple River bridges, respectively. By accounting for the rotations at the pile-abutment connection, the strains were reduced. The strains compared well with the experimental strains; the experimental values were bounded by the two soil idealizations.

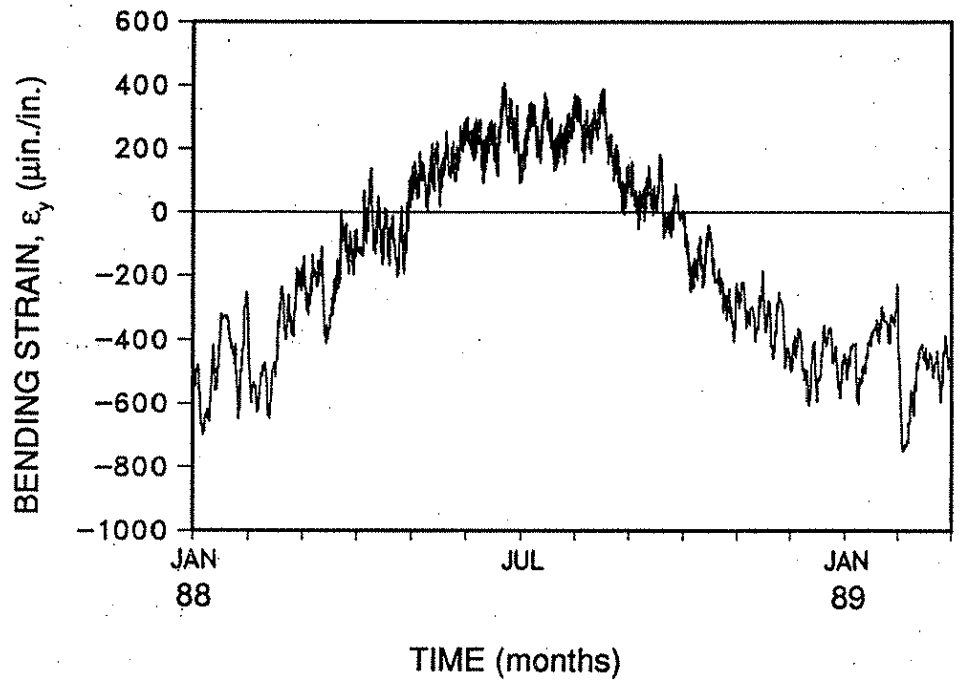

Fig. 4.5. Analytical weak axis strain at the Boone River Bridge. [Eq. (4.6) and L_{My} = 115 in. and L_{Hy} = 101 in.]

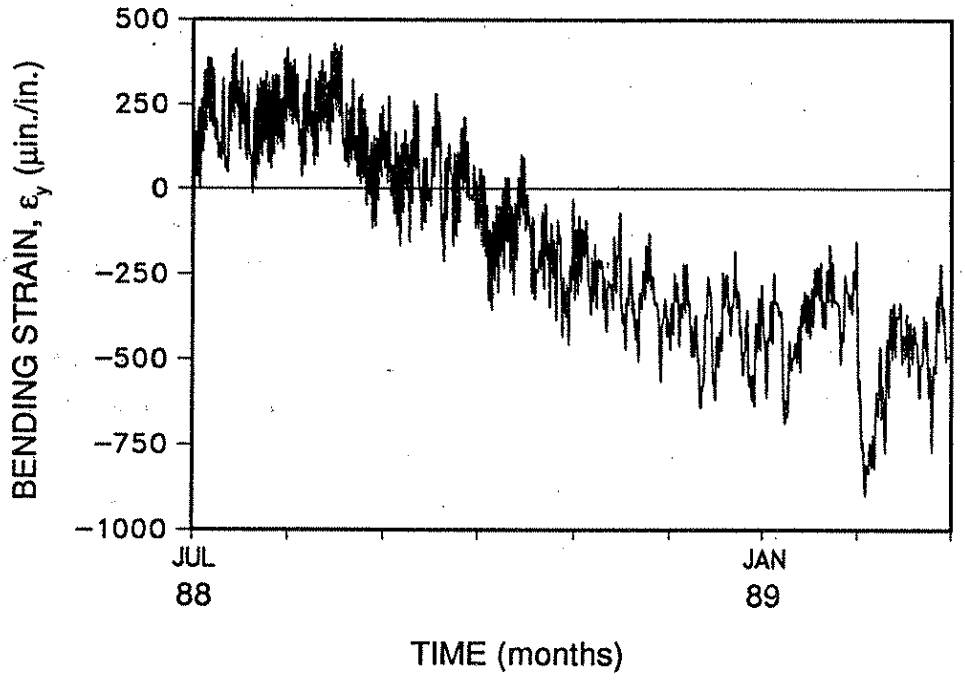

Fig. 4.6. Analytical weak axis strain at the Maple River Bridge. [Eq. (4.6) and L_{My} = 114 in. and L_{Hy} = 106 in.]

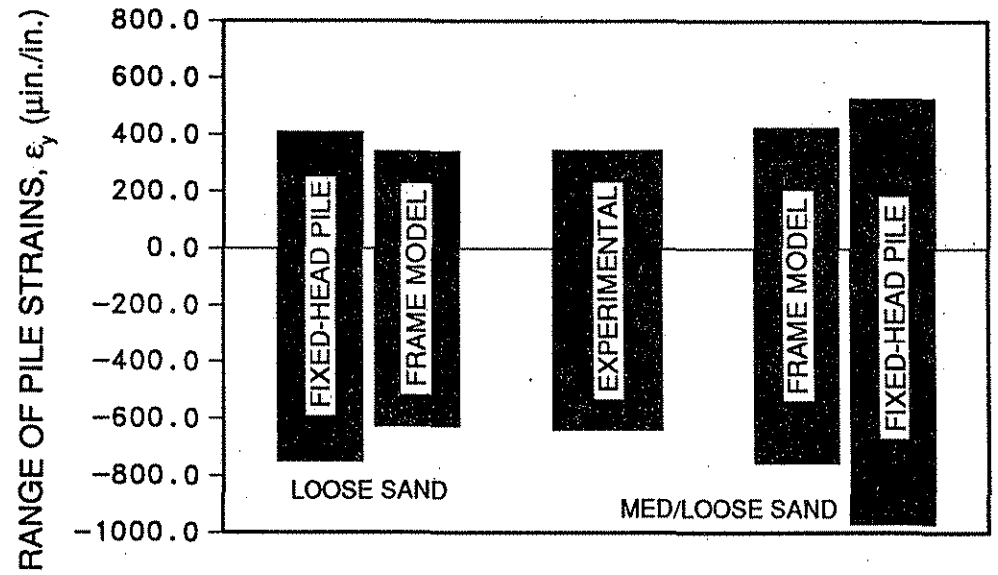

Fig. 4.7. Experimental and analytical weak axes strains for the Boone River Bridge.

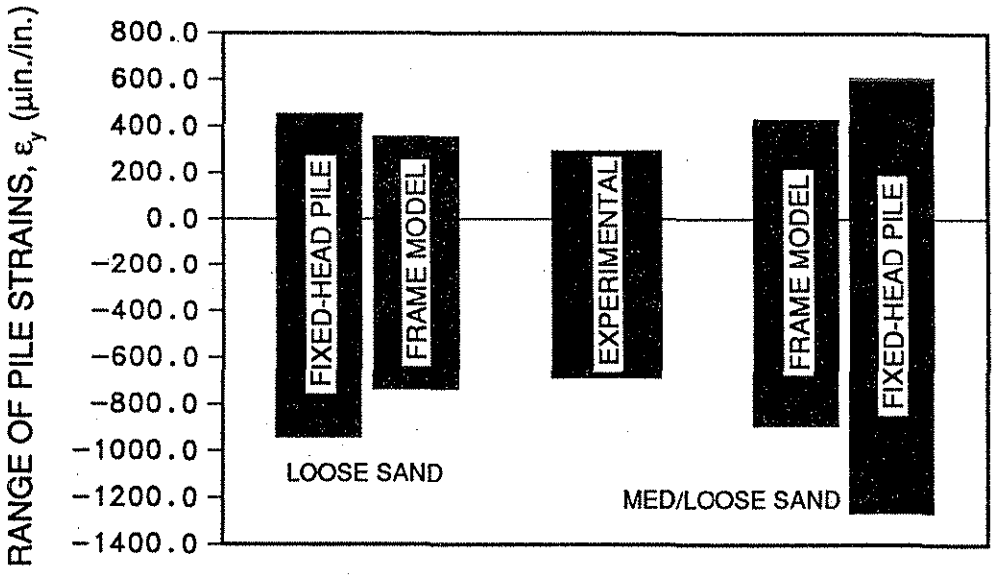

Fig. 4.8. Experimental and analytical weak axes strains for the Maple River Bridge.

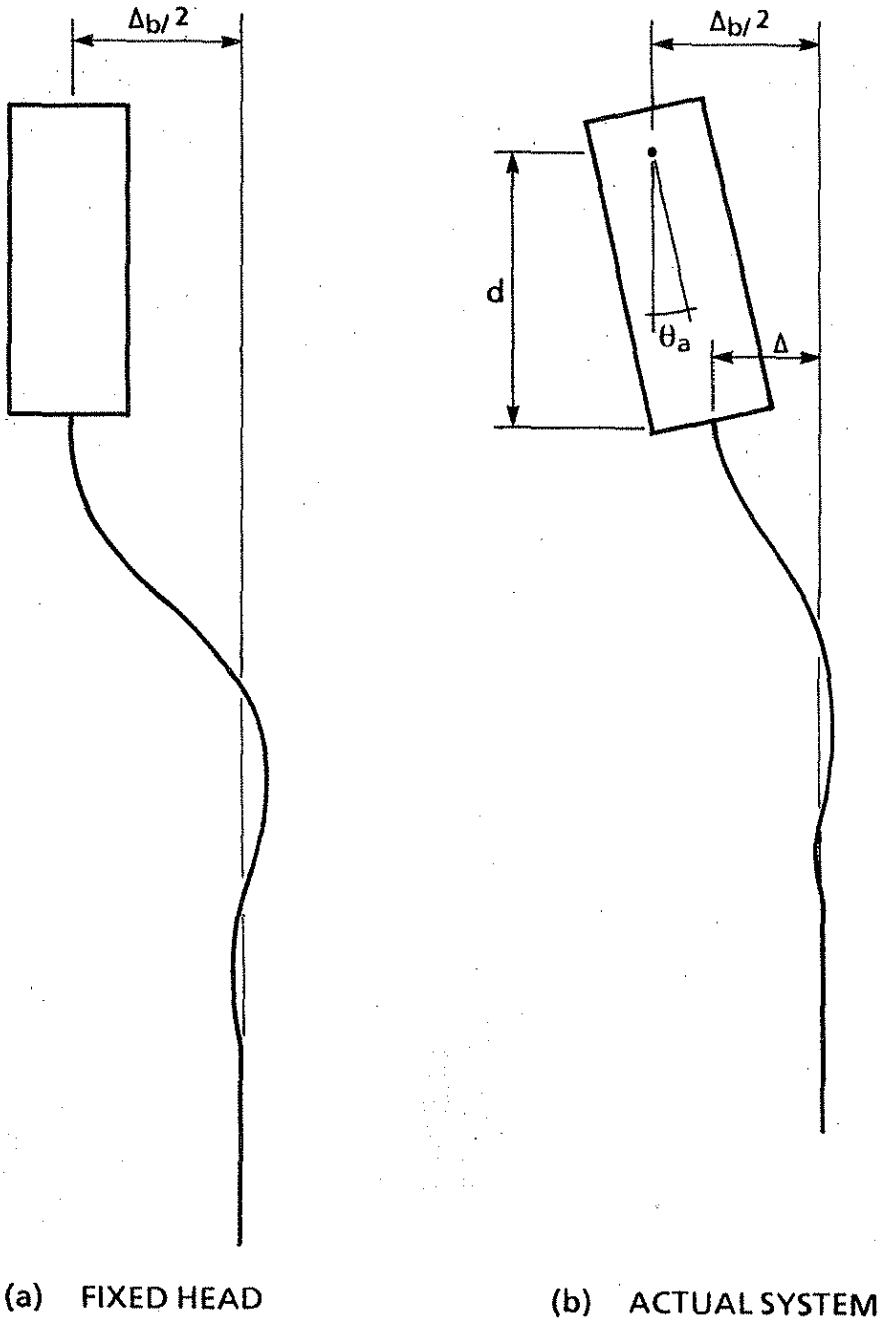

Fig. 4.9. Abutment-pile movement: (a) fixed head, (b) actual system with abutment rotation.

4.5. Pile Strains due to Lateral Movement

The experimental strains for strong axis bending, ε_x (shown in Figs. 2.17 and 2.18), indicate some lateral motion of the bridges as longitudinal thermal expansion and contraction occurred. The lateral displacements associated with lateral temperature expansion were small and were neglected. A lateral frame model was developed to predict these strains.

4.5.1. Soil Pressure

For the symmetrical skewed bridges to displace laterally, a lateral force is required. The passive soil behind and in front of the skewed abutment creates such a force (Fig. 4.10). The maximum passive force, P_n, which can be developed normal to the face of the abutment [28] is

$$P_n = \frac{1}{2} \gamma H^2 K_p B \tag{4.8}$$

where γ is the unit weight of the material surrounding the abutment, H and B are the height and skewed width of the abutment, respectively, and K_p is a coefficient of passive earth pressure

$$K_p = \frac{1 + \sin\phi}{1 - \sin\phi} \tag{4.9}$$

where ϕ is the internal friction angle of the soil. (Refer to Table 4.2 for typical values of γ and ϕ.) As the skewed bridge expands, a frictional force, P_t, will develop tangent to the soil-abutment interface (Fig. 4.9). The frictional force is limited to μP_n where μ is the coefficient of friction between the soil and the abutment. A typical value for μ is 0.4 [28]. The lateral soil force normal to the longitudinal bridge axis, P_x, corresponding to full passive pressure is

$$P_x = P_n (\sin\beta - \mu \cos\beta) \tag{4.10}$$

where β is the skew angle as shown in Fig. 4.10.

Spangler and Handy [28], Das [29], Terizaghi [30], and Clough and Duncan [31] pointed out that large abutment movements are required to develop the full passive pressure.

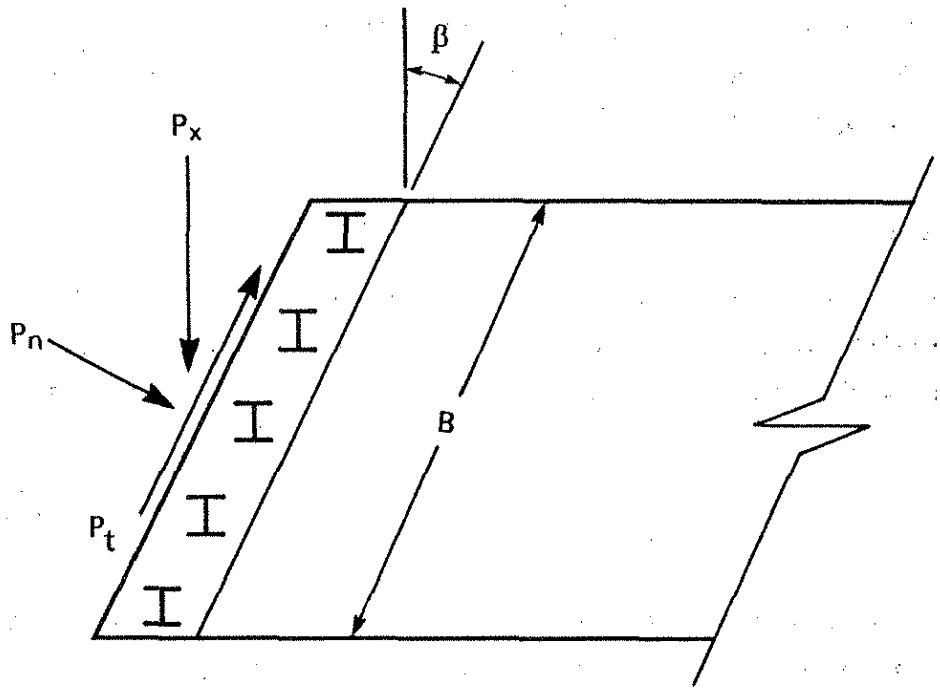

Fig. 4.10. Passive soil forces on skewed abutment.

Figure 4.11 [31] shows a curve relating the passive pressure to the wall movement for a particular retaining wall. All these authors state that there is much uncertainty in predicting passive pressures. According to Fig. 4.11, the passive pressure at the bridge sites could be any value between the full passive pressure, P_n, and the full active pressure. Bridge movement, soil moisture conditions, and time will all have an effect. For example, as the bridge expands and contracts, void spaces may be created between the soil and the abutment, which may affect the passive earth pressures. As with many soil problems, a reliable value is not available from elementary soil mechanics.

Using Eq. (4.8), we find the maximum passive forces are 800 kips and 560 kips at the Boone River and Maple River bridges, respectively. These values were obtained with a unit weight, γ, assumed to be 120 lb/ft^3 and a coefficient of passive earth pressure, K_p, of 3.69 (friction angle of 35°). The abutments were 8 and 8.5 ft in height at the Boone River and Maple River bridges, respectively; the abutment widths, B, were 56.6 and 34.6 ft, respectively. The skew angles, β, were 45° and 30° at the Boone River and Maple River bridges, respectively. The displacements required to develop these large maximum passive pressures are probably in the range of 2.5 to 3 in. (Fig. 4.11). The maximum experimental displacement ranges of 2 and 2 1/2 in. for the two bridges indicated that the maximum passive pressures were probably not reached, especially at the Boone River Bridge.

4.5.2. Lateral Frame Model

A lateral frame model was developed to predict both the strong axis pile strains, ε_x, and the lateral displacement of the skewed bridges. Figure 4.12 shows the two-dimensional model used for the frame analysis of the Maple River Bridge. Equivalent cantilevers were used to approximate the lateral pile behavior, as in the longitudinal frame model (Sec. 3.3), except strong axis properties were used (i.e., L_{Mx} from Table 4.3). The base of the equivalent cantilevers were fixed against lateral motion and rotation. Axial springs were inserted at the bottom of the equivalent cantilevers to approximate the axial shortening and slippage of the pile below L_{Mx}. The stiffness of the springs was assumed to be one-half the axial stiffness of the piles. In general, the stiffness depends on the surrounding soil–for example, the point springs, k_q, and vertical springs, k_v, given in Ref. [1]. The piles in the Maple River Bridge are battered at a slope of 3:1 (Fig. 2.4).

The lateral force, P_x, corresponding to full passive pressure (Eq. 4.11) was applied to the bridges (340 kips for the Boone River Bridge and 86 kips for the Maple River Bridge).

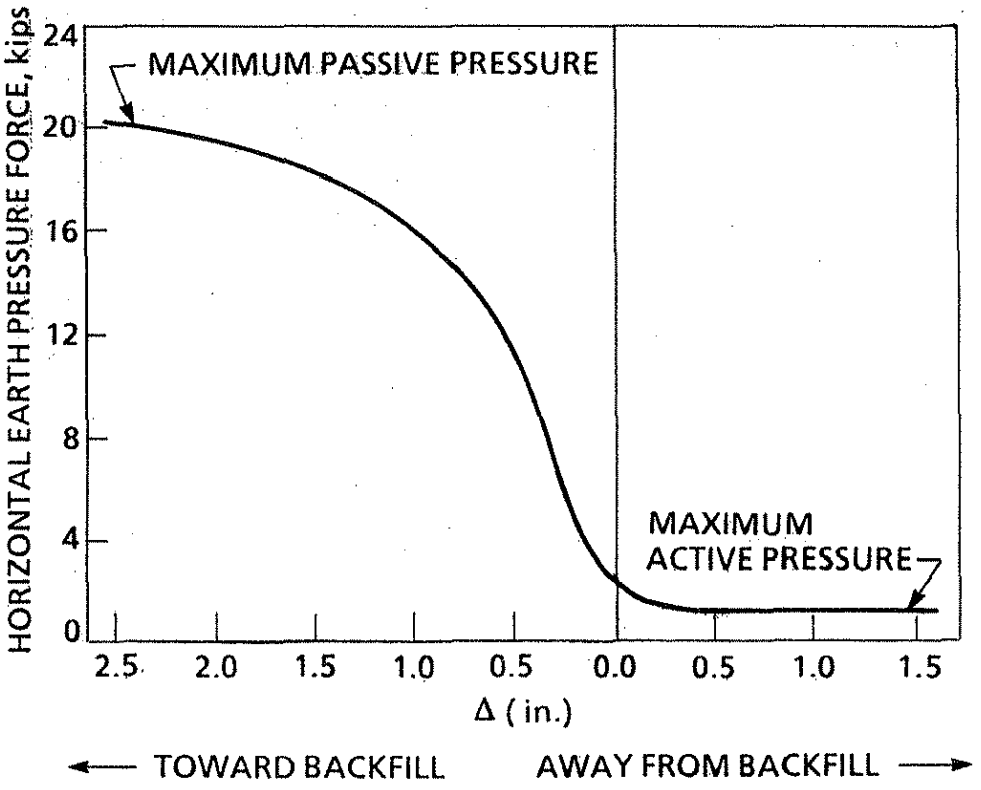

Fig. 4.11. Soil pressure behind a moving wall.

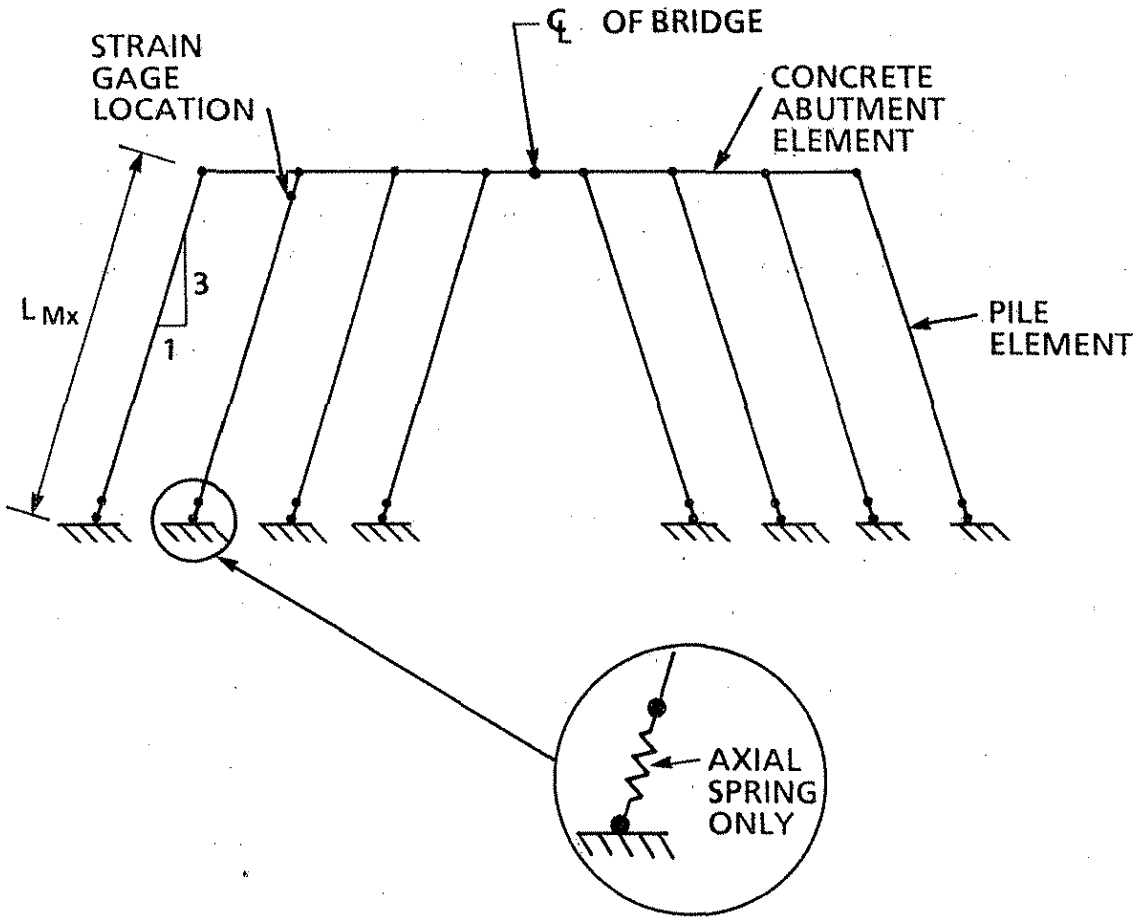

Fig. 4.12. Lateral frame model of Maple River Bridge.

The strong axes strains, ε_x, from the frame analysis corresponding to full passive pressure are 1300 μ in./in. at the Boone River Bridge and 407 μ in./in. at the Maple River Bridge. Obviously, the Boone River Bridge did not develop full passive pressure since experimental strains were of the order of 200 μ in./in. (Fig. 2.17). However, at the Maple River Bridge, the predicted ε_x strains due to the full passive pressure were only slightly larger than those measured (350 μ in./in.) in Ch. 2 (Fig. 2.18). Note that the Boone River Bridge, which is concrete, did not expand as much as the steel Maple River Bridge. With reference to Fig. 4.11, one would expect the passive pressures of the Boone River Bridge to be significantly smaller than at the Maple River Bridge.

4.6. Recommendations

The individual pile model gives conservative values of the weak axis pile strains, ε_y. A longitudinal frame analysis is recommended for these pile strain predictions. Strong axis pile strains, ε_x, due to the lateral movement of skew bridges can be significant and should be analyzed–for example, by the lateral frame model. The magnitude of the passive soil pressure on the abutment is uncertain. For purposes of design, one should assume full passive pressures unless a smaller value can be justified by rational methods even though this is very conservative for one of the bridges.

Careful consideration should be given to the soil properties. Soil properties at bridge sites should be quantified with standard penetration tests or other in-situ measurement devices. Bounding techniques illustrated in this chapter may be useful design tools.

5. DESIGN RECOMMENDATIONS AND EXAMPLE

5.1. Thermal Expansion Range

For design purposes, the coefficient of thermal expansion for bridges should be experimentally determined or predicted by some other means, such as Eq. (1.1). In lieu of these recommendations, AASHTO (Sec. 1.4.2) values for the coefficient of thermal expansion can be used. The recommended coefficients of thermal expansion for concrete for the Boone River and Maple River bridges are 0.0000045 and 0.000005 in./in. (°F) respectively.

The temperature ranges recommended for the design of bridges in Iowa are

	Temperature Range
Concrete Deck	150° F
Concrete and Steel Girders	140° F

Bridge longitudinal displacements can be predicted by the axial displacement model or by a longitudinal frame model (Fig. 3.7).

5.2. AASHTO Case A: Capacity of a Pile as a Structural Member [1]

5.2.1. Structural Analysis

The equivalent cantilevered idealization is sufficiently accurate for design purposes (Appendix C). Stresses due to bending caused by the thermal movements can be predicted by using a longitudinal frame model and a lateral frame model (Fig. 3.7 and Fig. 4.12). The simpler but more conservative fixed-head model in Ch. 4 can be used in lieu of the longitudinal frame model. Stresses due to lateral movement of skewed bridges should not be neglected. Unless a smaller value can be justified by analysis, full passive soil pressure should be assumed to act on the abutment.

5.2.2. Alternative One

Alternative One, which follows the AASHTO requirements, includes all the stresses induced by the thermal expansion and contraction of the bridge superstructure. Alternative One has no ductility requirements and is recommended for piles with limited or unknown ductility capacity.

5.2.3. Alternative Two

For Alternative Two, the flexural stresses induced in the pile because of thermal expansion are neglected. Alternative Two does account for the secondary moment effect (PΔ), which for a fixed-head pile (Fig. 4.4), is [1]

$$M = \frac{P\Delta}{2} \tag{5.1}$$

Alternative Two assumes that some plastic redistribution of forces will occur during the thermal movements, that is, a partial plastic hinge may occur in the pile. The ductility capacity of the pile must be sufficient to permit some inelastic rotation at the pile head. Ductility requirements for fixed-head steel H piles are satisfied if the pile head translations, Δ_x and Δ_y, are limited by [32]

$$\frac{\Delta_x}{\Delta_{ix}} + \frac{\Delta_y}{\Delta_{iy}} \leq 1 \tag{5.2}$$

in which

$$\Delta_{ix} = \Delta_{ox}(0.6 + 2.25\, C_i) \tag{5.3}$$

$$\Delta_{iy} = \Delta_{oy}(0.6 + 2.25\, C_i) \tag{5.4}$$

$$C_i = \frac{19}{6} - \frac{1}{30}\left(\frac{b_f}{2t_f}\right)\sqrt{F_y} \leq 1 \tag{5.5}$$

$$\Delta_{ox} = \frac{F_{bx}L_{Mx}^2}{3Ed} \tag{5.6}$$

$$\Delta_{oy} = \frac{F_{by}L_{My}^2}{3Eb_f} \tag{5.7}$$

where F_{bx} and F_{by} are the allowable bending stresses in the direction of the bending, d is the section depth, b_f is the flange width, F_y is the steel yield stress, and t_f is the flange thickness. (Refer to Ref. [32] for pinned-head case.)

In Alternative Two, limited straining beyond the yield point is permitted. Equation (5.2) limits inelastic rotations to about three times the elastic rotation [32]. For weak axis bending of an HP shape with an idealized elastic-plastic material, flexural strains up to six times yield can be expected at the flange tips. Fatigue at this strain level should not be a problem for the low number of cycles associated with annual thermal movements [33].

Alternative Two is not recommended for piles with limited or unknown ductility. The ductility capacity of timber or concrete piles has not been addressed.

5.3. AASHTO Case B: Capacity of a Pile to Transfer Load to Ground

Frictional capacities of piles can be affected by thermal expansion and contraction. Figure 5.1 (from Ref. [1]) shows the gap that may form between the soil and pile and reduce the frictional length by ℓ_n [1]. Figure 5.2 is used to find ℓ_n for a prescribed y_{max}, the limiting displacement below which the frictional capacity is unaffected. A suggested value of y_{max} is 2% of the pile diameter.

The gap shown in Fig. 5.1 is assumed not to affect the bearing capacity at the pile tip.

5.4. AASHTO Case C: Capacity of the Ground to Support Load

Thermal displacements are assumed not to affect the capacity of the soil to support the load.

5.5. Other Recommendations

Piles should be driven in oversized, predrilled holes and oriented such that bending occurs predominantly about the weak axis. These details help to increase the flexibility of the piles.

The properties of the surrounding soil should be investigated by soil borings and standard penetration tests to determine the lateral soil stiffness as accurately as possible.

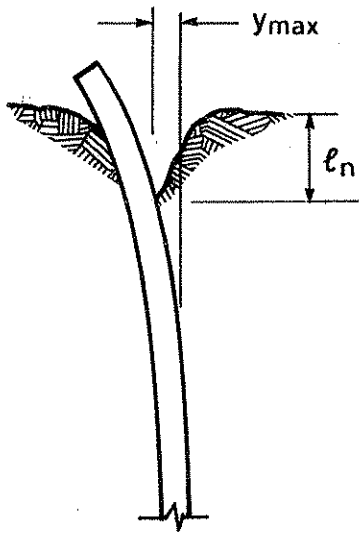

Fig. 5.1. Gap between the pile and the soil caused by cyclic horizontal movement.

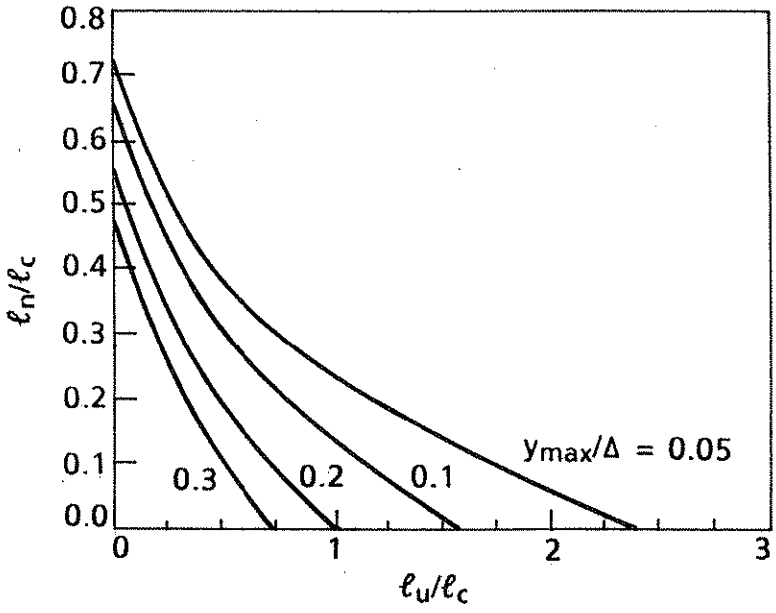

Fig. 5.2. Frictional length reduction for a fixed-head pile in uniform soil.

For skewed bridges, one should consider battering the piles in the lateral direction to limit lateral motion. Means of attenuating the passive soil pressure behind the abutment should be investigated. For example, if the passive pressure can be reduced by one-half with compressible materials behind the abutment, the strong axis strains will be reduced.

5.6. Design Example

The design recommendations are illustrated in an example to check the adequacy of the Maple River Bridge abutment piles. The Maple River Bridge is a three-span, four steel girder structure approximately 320 ft long (refer to Sec. 2.2.1 and Figs. 2.5 to 2.7). The bridge has a skew of 30°. Eight HP 10x42 steel piles (F_y of 36 ksi) were placed 4 ft-11 in. apart. The piles were driven into 12-ft-deep oversized, predrilled holes that were filled with loose sand and oriented with bending occurring primarily about the weak axis (Fig. 2.4). The piles, which are battered in the lateral direction at a slope of 3:1, are 55 ft long and have a specified minimum bearing load of 32 tons.

5.7. Structural Analysis

The AASHTO *Standard Specifications for Highway Bridges* [5] requires that displacements or stresses caused by thermal expansion and contraction be considered in design [5, Sec. 3.16]. Section 3.22 in the AASHTO specifications gives several load groups that include temperature effects. Only Load Group IV will be considered in this design example. The terms included in Group IV are dead load (D), live load (L), impact (I), and temperature (T). A 25% increase in allowable stress is permitted by AASHTO for Load Group IV [5, Table 3.22. 1A].

5.7.1. Structural Model

The longitudinal frame model presented in Ch. 3 was used to predict the weak axis bending stress, f_{by}, in the pile. The lateral frame model presented in Ch. 4 was used to predict the strong axis bending stress, f_{bx}, due to lateral motion. The equivalent cantilevered lengths for piles in loose sand (Table 4.3) were used.

5.7.2. Vertical Loading

The determination of stresses for vertical loading (dead load, live load, and impact) were not within the scope of this research project. For purposes of this example, suppose the axial and bending stresses because of vertical load, f_{aV} and f_{byV}, respectively, are

$$f_{aV} = 4.2\ ksi \tag{5.8}$$

$$f_{byV} = 7.1\ ksi \tag{5.9}$$

The strong axis bending stress, f_{bxV}, will be neglected. In the usual situation, these stresses would be calculated as the bridge was being designed for vertical load.

5.7.3. Thermal Loading

Uniform temperatures of $\pm 75°$ F for the deck and $\pm 70°$ F for the girders were used for design. Full passive pressure was applied to the abutment at two-thirds of the way down in the longitudinal frame model. The resulting longitudinal displacements, Δ_y, were calculated to be 0.78 in. from the axial model (Eq. 3.5) and 0.73 in. from the longitudinal frame model. The small difference between the two models was due to the small abutment rotation (Fig. 4.9).

The axial stress from the frame model, f_{aT}, was 0.6 ksi. The weak axis bending stress predicted by the longitudinal frame model (Fig. 3.7) was

$$f_{byT} = 26.9\ ksi \tag{5.10}$$

[The axial model (Eq. 4.6) predicted higher bending stresses (29.8 ksi) because it neglected the rotation of the abutment.]

The strong axis bending stress from the lateral frame model (Fig. 4.12) was

$$f_{bxT} = 11.8\ ksi \tag{5.11}$$

Remember that this stress is conservative since it corresponds to the full passive pressure, which probably was not reached (Ch. 4). The lateral displacement corresponding to full passive pressure, Δ_x, was 0.30 in.

The total stresses for Load Group IV were

$$f_a = f_{aV} + f_{aT} = 4.8\ ksi \tag{5.12}$$

$$f_{by} = f_{byV} + f_{byT} = 34.0\ ksi \tag{5.13}$$

$$f_{bx} = f_{bxT} = 11.8\ ksi \tag{5.14}$$

5.8. Comparison with AASHTO Allowable Stresses

5.8.1. Case A

The capacity of the pile as a structural member (Case A) was checked using the AASHTO Service Load Design interaction equations [5, Eqs. (10-41) and (10-42)].

The allowable axial stress, F_a, is 19.5 ksi [5, Table 10.32.1A], with K_y equal to 0.65 [5, Table C-1], L_{By} of 187 in. (Table 4.3), r_y equal to 2.41 in., and a 25% allowable stress increase [5, Table 3.22.1A]. The corresponding elastic buckling stress, F'_{ey}, for weak axis bending, is 66.3 ksi [5, Eq. (10-43)], which also includes a 25% increase. For strong axis bending, F'_{ex} is 165.3 ksi [5, Eq. (10.43)], with K_x equal to 0.65, an L_{Bx} of 203 in. (Table 4.3), r_x equal to 4.13 in., and a 25% increase.

An HP 10x42 steel pile is not a compact section with respect to the flanges. (The $b_f/2t_f$ of 12 is between $65/\sqrt{F_y}$ and $95/\sqrt{F_y}$ for F_y of 36 ksi.) For such a case, AISC [34] presents an equation for the allowable stress with weak axis bending [34, Eq. (1.5–5b)]. Decreasing the AISC allowable by the ratio 0.55/0.66 (the nominal AASHTO allowable to the nominal AISC allowable) gives

$$F_{by} = F_y\left[0.896 - 0.0042\left(\frac{b_f}{2t_f}\right)\sqrt{F_y}\right] \tag{5.15}$$

or, for an HP 10x42 with thermal loading,

$$F_{by} = 36\ ksi[0.896 - 0.0042(12)\sqrt{36\ ksi}\ ](1.25) = 26.7\ ksi \tag{5.16}$$

For strong axis bending, AISC [34, Eq. (1.5-5a)] is also decreased by the ratio 0.55/0.66 to give

$$F_{bx} = F_y \left[0.658 - 0.0017 \left(\frac{b_f}{2t_f} \right) \sqrt{F_y} \right] \tag{5.17}$$

which, for an HP 10x42, gives

$$F_{bx} = 36\ ksi [0.658 - 0.0017(12)\sqrt{36}\,](1.25) = 24.1\ ksi \tag{5.18}$$

Alternative One

It was apparent that Alternative One would not be satisfied since the applied bending stress, f_{by}, of 34.0 ksi is greater than the allowable bending stress of 26.7 ksi. (This adds evidence to the observation in Sec. 2.3.5 that yielding probably occurred during the experimental data collection.) However, the stability and yield equations will be illustrated for completeness. The stability equation is [5, Eq. (10-41)]

$$\frac{f_a}{F_a} + \frac{C_{mx} f_{bx}}{\left[1 - \dfrac{f_a}{F'_{ex}} \right] F_{bx}} + \frac{C_{my} f_{by}}{\left[1 - \dfrac{f_a}{F'_{ey}} \right] F_{by}} \leq 1.0 \tag{5.19}$$

and the yield equation is [5, Eq. (10-42)]

$$\frac{f_a}{0.472 F_y} + \frac{f_{bx}}{F_{bx}} + \frac{f_{by}}{F_{by}} \leq 1.0 \tag{5.20}$$

The quantities C_{my} and C_{mx} equal 0.85 [34, Sec. 1.6.1] since both ends of the pile were restrained and transverse loads (soil pressures) existed. Substituting the appropriate values into these equations gives

$$\frac{4.8\ ksi}{19.5\ ksi} + \frac{0.85\,(11.8\ ksi)}{\left[1 - \frac{4.8\ ksi}{165.3\ ksi}\right](24.1\ ksi)} + \frac{0.85\,(34.0\ ksi)}{\left[1 - \frac{4.8\ ksi}{66.3\ ksi}\right](26.7\ ksi)} = 1.84 > 1.0 \qquad (5.21)$$

and

$$\frac{4.8\ ksi}{0.472\,(36\ ksi)\,1.25} + \frac{11.8\ ksi}{24.1\ ksi} + \frac{34.0\ ksi}{26.7\ ksi} = 1.99 > 1.0 \qquad (5.22)$$

As expected, the design would be inadequate if Approach One were used.

Alternative Two

With an axial pile load of 59.5 kips [4.8 ksi, Eq. (5.12)], a Δ_y of 0.73 in. (Sec. 3.3), and a Δ_x of 0.30 in. (Sec. 5.7.3), the secondary bending stresses due to thermal movement by Eq. (5.1) are

$$f_{byT} = \frac{59.5\ kips\,(0.73\ in.)}{2(14.2\ in.^3)} = 1.5\ ksi \qquad (5.23)$$

and

$$f_{bxT} = \frac{59.5\ kips\,(0.30\ in.)}{2(43.4\ in.^3)} = 0.2\ ksi \qquad (5.24)$$

Checking the stability equation, including the vertical load stresses (Eq. 5.8 and 5.9), gives

$$\frac{4.8\ ksi}{19.5\ ksi} + \frac{0.85\,(0.2\ ksi)}{\left[1 - \frac{4.8\ ksi}{165.3\ ksi}\right](24.1\ ksi)} + \frac{0.85\,(7.1 + 1.5)\ ksi}{\left[1 - \frac{4.8\ ksi}{66.3\ ksi}\right](26.7\ ksi)} = 0.55 < 1.0 \qquad (5.25)$$

and the yield equation

$$\frac{4.8\ ksi}{0.472\,(36\ ksi)\,1.25} + \frac{0.2\ ksi}{24.1\ ksi} + \frac{(7.1 + 1.5)\ ksi}{26.7\ ksi} = 0.56 < 1.0 \qquad (5.26)$$

The design thus satisfies the stress criteria of Alternative Two.

The inelastic rotational capacity reduction factor, C_i (Eq. 5.5), is

$$C_i = \frac{19}{6} - \frac{1}{30}(12)\sqrt{36.0\ ksi} = 0.77 < 1.0 \tag{5.27}$$

and the lateral displacements, Δ_{oy} and Δ_{ox}, are

$$\Delta_{oy} = \frac{26.7\ ksi\,(114\ in.)^2}{3(29000\ ksi)\,(10.075\ in.)} = 0.40\ in. \tag{5.28}$$

and

$$\Delta_{ox} = \frac{24.1\ ksi\,(144\ in.)^2}{3(29000\ ksi)\,(9.70\ in.)} = 0.59\ in. \tag{5.29}$$

The unidirectional allowable displacements (Eq. 5.3 and 5.4) are

$$\Delta_{iy} = 0.40\ in.\,[0.6 + 2.25(0.77)] = 0.93\ in. \tag{5.30}$$

$$\Delta_{ix} = 0.59\ in.\,[0.6 + 2.25(0.77)] = 1.38\ in. \tag{5.31}$$

Substituting into the biaxial ductility criterion (Eq. 5.2) gives

$$\frac{0.73\ in.}{0.93\ in.} + \frac{0.30\ in.}{1.37\ in.} = 1.004 \simeq 1.0 \tag{5.32}$$

Therefore, the ductility criterion was satisfied and the design satisfies the requirements of Alternative Two.

5.8.2. Case B

Case B (capacity of the pile to transfer load to ground) is checked by verifying that the frictional capacity of the pile is adequate if the length, ℓ_n, is deducted (Fig. 5.2). The length, ℓ_n, is controlled by y axis bending in this case. If the sand in the predrilled hole is considered, ℓ_u/ℓ_c equals zero. With y_{max}/Δ_y equal to 0.2 in./0.73 in. or 0.275, Fig. 5.2 gives an ℓ_n of 0.5 ℓ_{cy}. With ℓ_{cy} equal to 13.6 ft, ℓ_n becomes 6.8 ft. This implied that y_{max} occurred within the sand of the predrilled hole. Most likely, the entire 12 ft of loose sand in the predrilled hole was neglected in the pile design. Hence, no additional deduction for lateral movement is necessary and Case B is satisfied.

5.8.3. Case C

Thermal displacements were assumed not to affect Case C (capacity of ground to support the load).

5.8.4. Design Adequacy

Since the pile met all criteria of Alternative Two, the pile design was deemed satisfactory for the Maple River Bridge. The bridge could be no longer since the ductility criteria (Eq. 5.32) was just satisfied. [The stability and yield equations (5.25) and (5.26) do not control.] Because of a reduced coefficient of thermal expansion, concrete bridges could be longer. If the passive pressure behind the abutment could rationally be reduced for design purposes, a longer steel bridge could be permitted.

6. SUMMARY, CONCLUSIONS, AND RECOMMENDATIONS FOR FURTHER WORK

6.1. Summary

The objective of this research was to verify a design procedure for piles in integral abutment bridges with experimental data from two bridges. Thus, refined design recommendations are made, based on the results of this work.

The field tests (Ch. 2) consisted of instrumenting two skewed bridges in Iowa. The experimental data consisted of air temperatures, bridge temperatures, bridge displacements, and pile strains. In addition, concrete core samples were collected from the bridges and laboratory measurements of the coefficient of thermal expansion were made. Measured coefficients of thermal expansion were significantly below AASHTO values.

An axial displacement model (Ch. 3) was developed to predict the longitudinal thermal movements of the two bridges. The bridges were subdivided into segments, each with uniform temperature, coefficient of thermal expansion, and modulus of elasticity. A longitudinal frame model that included abutment rotations was also used to determine the longitudinal thermal displacements. The temperature ranges recommended for the deck and girders differ from the AASHTO values, especially for concrete bridges.

An equivalent cantilevered model (Ch. 4) was used to predict the strains in the piles. When the pile head was assumed to be fixed, the model was conservative when compared to the measured strains. The longitudinal frame model in Ch. 3, which permitted abutment rotations, gave better predictions of weak axis strains. The lateral frame model in Ch. 4 was used to predict the strong axis strains as well as the lateral movements. Full passive soil pressures were assumed.

Design recommendations for temperature ranges and coefficients of thermal expansion are summarized in Ch. 5. Two alternative approaches, which depend upon the ductility capacity of the pile, are recommended for designing piles as structural members. Recommendations on pile orientation, predrilled holes, and skewed bridges are also given. Chapter 5 concludes with a design example.

6.2. Conclusion

The recommendations, which are summarized in Ch. 5, should be followed for the design of piles in integral abutment bridges.

The coefficients of thermal expansion of concrete, the bridge temperature range, and the effects of the passive earth pressures are important parameters that affect the maximum safe length of integral abutment bridges.

6.3. Recommendations for Further Work

Other studies that were not addressed in this report but may deserve further consideration include:

(1) Lateral displacements of skew bridges.

(2) The ductility of timber and concrete piles.

(3) The effects of longitudinal displacements on the approach slab and backfill material.

(4) The passive and active soil pressures both behind and in front of the abutment.

7. REFERENCES

1. Greimann, L. F., Abendroth, R. E., Johnson, D. E., and Ebner, P. B. "Pile Design and Tests for Integral Abutment Bridges." Final Report, Iowa DOT Project HR-273, ISU-ERI-Ames 88060, Dec. 1987.
2. Greimann, L. F., Wolde-Tinsae, A. M., and Yang, P. -S. "Skewed Bridges with Integral Abutments." *Transportation Research Record* 903, Transportation Research Board, National Academy of Sciences, Washington, D.C., 1983, pp. 64–72.
3. Greimann, L. F., Yang, P. -S., Edmunds, S. K., and Wolde-Tinsae, A. M. "Design of Piles for Integral Abutment Bridges." Final Report, Iowa DOT Project HR-252, ISU-ERI-Ames 84286, Aug. 1984.
4. U.S. Department of Transportation, Federal Highway Administration. "Integral, No-Joint Structures and Required Provisions for Movement." T5140.13, Jan. 28, 1980.
5. American Association of State Highway and Transportation Officials. *Standard Specifications for Highway Bridges*, 13th ed. Washington, D.C.: American Association of State Highway and Transportation Officials, 1983.
6. Wolde-Tinsae, A. M., Greimann, L. F., and Yang, P. -S. "Nonlinear Pile Behavior in Integral Abutment Bridges." Iowa DOT Project HR-227, ISU-ERI-Ames-82123, Feb. 1982.
7. Greimann, L. F., Yang, P. -S., and Wolde-Tinsae, A. M. "Nonlinear Analysis of Integral Abutment Bridges." *Journal of Structural Engineering*, ASCE, Vol. 112, No. 10, Oct. 1986, pp. 2263–2280.
8. Yang, P. -S., Wolde-Tinsae, A.M., and Greimann, L. F. "Nonlinear Finite Element Study of Piles in Integral Abutment Bridges." Iowa DOT Project HR-227, ISU-ERI-Ames-83068, Sept. 1982.
9. Jorgenson, J. L. "Behavior of Abutment Piles in an Integral Abutment in Response to Bridge Movements." *Transportation Research Record* 903, Transportation Research Board, National Academy of Sciences, Washington, D.C., 1983, pp. 72–79.
10. Lee, H. W., and Sarsam, M. B. "Analysis of Integral Abutment Bridges." South Dakota Department of Highways, Pierre, S.D., March 1973.
11. Imbsen, R. A., Vandershaf, D. E., Schamber, R. A., and Nutt, R. V. "Thermal Effects in Concrete Bridge Superstructures." *National Cooperative Highway Research Program Report* 276, Transportation Research Board, National Research Council, Washington, D.C., Sept. 1985.
12. Emanuel, J. H., and Hulsey, J. L. "Temperature Distributions in Composite Bridges." *Journal of the Structural Division*, ASCE, Vol. 104, No. ST1, Jan. 1978, pp. 65–78.
13. Churchward, A., and Sokal, Y. J. "Prediction of Temperatures in Concrete Bridges." *Journal of the Structural Division*, ASCE, Vol. 107, No. ST11, Nov. 1981, pp. 2163–2176.
14. Reynolds, J. C., and Emanuel, J. H. "Thermal Stresses and Movements in Bridges." *Journal of the Structural Division*, ASCE, Vol. 100, No. ST1, Jan. 1974, pp. 63–78.
15. Prakash Rao, D. S. "Temperature Distributions and Stresses in Concrete Bridges." *ACI Journal, Proceedings*, Vol. 83, No. 4, July-Aug. 1986, pp. 588–596.

16. Kennedy, J. B., and Soliman, M. H. "Temperature Distribution in Composite Bridges." *Journal of Structural Engineering*, ASCE, Vol. 113, No. 3, March 1987, pp. 475–482.

17. Soliman, M., and Kennedy, J. B. "Simplified Method for Estimating Thermal Stresses in Composite Bridges." *Transportation Research Record* 1072, Transportation Research Board, National Research Council, Washington, D.C., 1986, pp. 23–31.

18. Hulsey, J. L., and Emanuel, J. H. "Environmental Stresses in Flexibly Supported Bridges." *Transportation Research Record* 664, Transportation Research Board, National Academy of Sciences, Washington, D.C., 1978, pp. 262–270.

19. Radolli, M., and Green, R. "Thermal Stress Analysis of Concrete Bridge Superstructures." *Transportation Research Record* 607, Transportation Research Board, National Academy of Sciences, Washington, D.C., 1976, pp. 7–13.

20. Rahman, F., and George, K. P. "Thermal Stress Analysis of Continuous Skew Bridge." *Journal of the Structural Division*, ASCE, Vol. 105, No. ST7, July 1979, pp. 1525–1541.

21. Rhodes, J. A. "Thermal Properties." *Significance of Tests and Properties of Concrete and Concrete-Making Materials*, Special Technical Publication 1698, ASTM, 1978.

22. Davis, R. E. "A Summary of the Results of an Investigation Having To Do with Volumetric Changes in Cements, Mortars and Concretes, Due to Causes Other than Stress." *ACI Journal, Proceedings*, Vol. 26, No. 4, Feb. 1930, pp. 407–443.

23. Callan, E. J. "Thermal Expansion of Aggregates and Concrete Durability." *ACI Proceedings*, Feb. 1952, pp. 485–504.

24. Griffith, J. H. "Thermal Expansion of Typical American Rocks." Bulletin No. 128, Engineering Experiment Station, Iowa State College, Ames, Iowa, 1936, pp. 1–36.

25. Meyers, S. L. "Thermal Expansion Characteristics of Hardened Cement Paste and of Concrete." Highway Research Board, 1950, pp. 193–203.

26. Zuk, W. "End-Movement Studies of Various Types of Highway Bridges." *Highway Research Record* 295, Highway Research Board, National Research Council, Washington, D.C., 1969, pp. 1–4.

27. Emanuel, J. H., and Hulsey, J. L. "Prediction of the Thermal Coefficient of Expansion of Concrete." *Journal of the American Concrete Institute*, Vol. 74, No. 4, April 1977, pp. 149–155.

28. Spangler, M. G., and Handy, R. L. *Soil Engineering*, 4th Ed. New York: Harper and Row Publishers, Inc., 1982.

29. Das, B. M. *Principles of Foundation Engineering*. Boston: PWS-Kent Publishing Co., 1984.

30. Terizaghi, K. *Soil Mechanics in Engineering Practice*. New York: Wiley, Inc., 1967.

31. Clough, G. W., and Duncan, J. M. "Finite Element Analysis of Retaining Wall Behavior." *Journal of the Soil Mechanics and Foundations Division*, ASCE, Vol. 97, No. SM12, Dec. 1971, pp. 1657–1673.

32. Abendroth, R. E., and Greimann, L. F. "A Rational Design Approach for Integral Abutment Bridge Piles." accepted for publication in *Journal of the Structural Division*, ASCE, expected 1990.

33. Massonnet, C. E., and Save, M. A. *Plastic Analysis and Design, Vol. 1–Beams and Frames.* New York: Blaisdell Publishing Co., 1965, p. 35.

34. *Manual of Steel Construction,* 8th Ed. Chicago: American Institute of Steel Construction, Inc., 1980.

8. ACKNOWLEDGMENTS

This report was sponsored by the Iowa Department of Transportation, Highway Division, through the Iowa Highway Research Board.

The authors would like to thank the Woodbury County engineer, Lloyd Kallsen, and the Public Works Director of Webster City, Greg Malmstrom, for allowing us to use their bridges as experimental sites.

William Lundquist and Henry Gee at the Iowa Department of Transportation have supported our work and we thank them for that.

Thanks go out to Craig Hawkinson, an undergraduate Civil Engineering student, for his assistance with the field work and data reduction.

APPENDIX A: FIELD TESTS AND DATA REDUCTION

A.1. Development

A.1.1. Site Description

Chapter 2, Section 2.2 describes the locations of the two experimental sites. Soil borings were taken at each site. Figures 2.1 and 2.5 (Boone River and Maple River bridges, respectively) show the locations of the borings. The soil boring logs near the abutments are shown in Figs. A.1 and A.2 (Boone River and Maple River sites).

A.1.2. Instrumentation

Linear variable differential transformers (LVDTs) were used to monitor the bridge displacements. The displacement was calculated within the Micrologger 21X by first measuring two voltage measurements–one of normal polarity and the other reversed polarity. The two values were subtracted and the difference was used to calculate the displacement. Each LVDT was calibrated in the laboratory to determine the multiplier.

The thermocouples consisted of two types of wire leads: copper and constantan. The two leads were soldered together at the location where the temperature was to be measured. At the Micrologger 21X, the copper lead was connected to the high input of the differential channel and the constantan lead was connected to the low input. The Micrologger 21X measured the differential voltage across the two leads. The measurement was then converted to degrees Fahrenheit.

Two piles were instrumented with four electrical-resistance strain gages to monitor strains just below the abutment. The gages were 120-ohm resistor. The strain gages were placed on the outside faces of the flanges and located 1 3/4 in. in from the flange tips. The strain gages were bonded to the pile using AE10/15 epoxy, which has good ductility characteristics over the range of temperatures encountered in the field. Various protective measures were taken to seal the gages from the environment. A foil covering was placed over the gages to reduce electrical interference. Two rubber compound coatings were placed over the gages. The first coating was a polysulfide liquid polymer compound, purchased from Measurements Group, Inc., and the second coating, a silicon-based metal sealer purchased from a local hardware store. Both were used to protect the entire installation from moisture contamination.

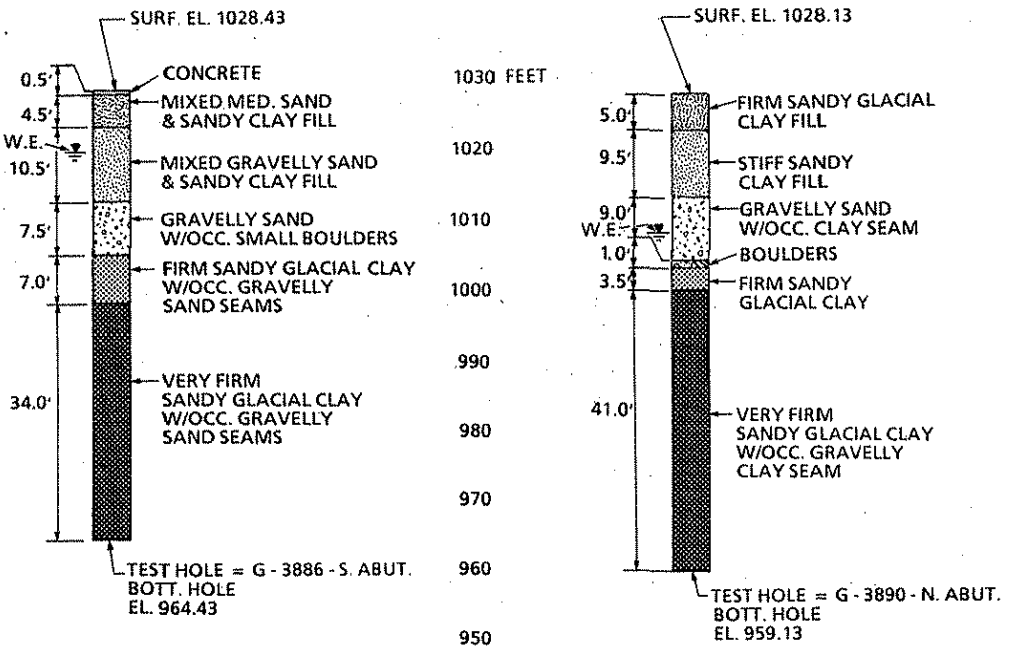

Fig. A.1. Boone River soil boring logs.

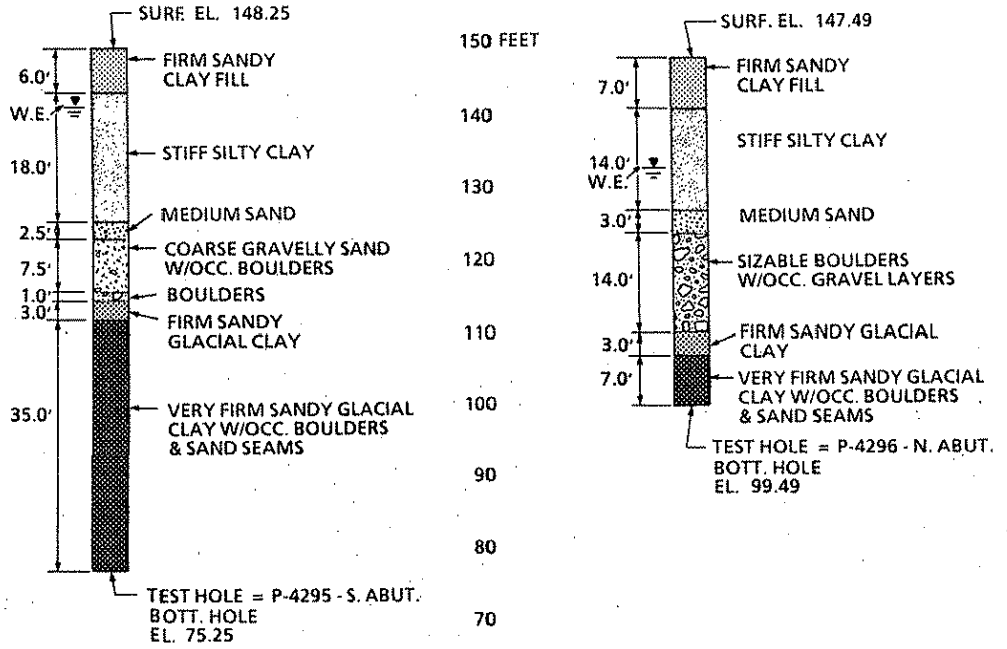

Fig. A.2. Maple River soil boring logs.

Completion cards were purchased from Campbell Scientific, Inc., to make the full bridge. The completion cards consisted of three precision resistors–a 120-ohm and two 1K ohm resistors–each having a 0.01% resistance tolerance and a 5ppm temperature coefficient.

Strains were measured by applying an excitation voltage to the full bridge and recording the differential voltage as the bridge output. The resulting value was converted to strain.

A.1.3. Micrologger 21X Program

The programs were written into the Micrologger 21X following the instructions given in the Campbell Scientific, Inc., *Operator's Manual.*

A.2. Data Reduction

A.2.1. General

Micrologger readings were recorded every 10 min and stored temporarily. An average was taken of the six 10-min readings every hour. The Micrologger 21X stored the experimental hourly average into final memory locations until a transfer was made from the 21X memory to cassette tapes. About every two weeks the data were downloaded to cassette tapes. At Iowa State University the data were uploaded to floppy disks and microcomputers were used to separate the LVDT and thermocouple data from the strain data. The data were then uploaded to a mainframe computer (Iowa State University VAX) for a more efficient means of data reduction. The LVDT data were converted to measured displacements using Eq. (2.1) in Ch. 2.

A.2.2. Strain Reduction

Strains were measured at four points at one vertical location on the pile near the abutment-pile connection (Fig. 2.9). The total strains were separated into four components: axial strain (ε_a), strain due to bending about the x (ε_x) and y (ε_y) axes, and strain due to torsional bending (ε_t). The four simultaneous equations, which state that the total strain at each gage location, ε_i, is the algebraic sum of the four strain components are

$$\varepsilon_1 = \varepsilon_a + \varepsilon_x + \varepsilon_y + \varepsilon_t \tag{A.1}$$

$$\varepsilon_2 = \varepsilon_a + \varepsilon_x - \varepsilon_y - \varepsilon_t \tag{A.2}$$

$$\varepsilon_3 = \varepsilon_a - \varepsilon_x - \varepsilon_y + \varepsilon_t \tag{A.3}$$

$$\varepsilon_4 = \varepsilon_a - \varepsilon_x + \varepsilon_y - \varepsilon_t \tag{A.4}$$

With ε_i given by the recorded data, the four equations were solved simultaneously for ε_a, ε_x, ε_y, and ε_t. The solution for the strains, ε_y and ε_x, is

$$\varepsilon_y = \frac{\varepsilon_1 - \varepsilon_2 - \varepsilon_3 + \varepsilon_4}{4} \tag{A.5}$$

$$\varepsilon_x = \frac{\varepsilon_1 + \varepsilon_2 - \varepsilon_3 - \varepsilon_4}{4} \tag{A.6}$$

As stated in Ch. 2, the ε_a and ε_t were small and neglected.

At the Maple River Bridge, gage 2 was not active and Eq. (A.2) is not usable. By neglecting the torsional strain in Eqs. (A.1), (A.3), and (A.4), one finds

$$\varepsilon_y = \frac{-\varepsilon_3 + \varepsilon_4}{2} \tag{A.7}$$

$$\varepsilon_x = \frac{-\varepsilon_1 + \varepsilon_3}{2} \tag{A.8}$$

Equations (A.5) through (A8) were used in Ch. 2 to calculate the experimental strains shown in Figs. 2.15 through 2.18.

APPENDIX B: EFFECTIVE COEFFICIENT OF THERMAL EXPANSION

B.1. Development

B.1.1. Test Samples

Three concrete cores were collected from the abutments at each of the two bridge sites for laboratory testing. The cores, of approximately 4 in. diameter, varied from 10 to 13 in. after trimming. Stainless steel studs were placed in the ends of the cores to hold the core in place while testing.

Before testing, the cores were subjected to three different moisture conditions. One core was placed in an oven (fully dry), another core was placed in a water bath (100% saturated), and the third core was left as an air-dried sample.

B.1.2. Testing System

Tests were conducted in an environmental chamber (see Fig. B.1), which was capable of controlling the temperature and moisture condition of each sample while monitoring the change in length and internal temperature of the core sample. The chamber consisted of a 13-in.-long piece of steel pipe with an inside diameter of 5 in. Insulation, consisting of 2-in.-thick styrofoam, was placed around the outside of the steel pipe to help control the temperature and humidity of the cores during testing. End caps were also used to seal the chamber.

The extensometer consisted of two boron nitride rods and an LVDT located at the top of the chamber (see Fig. B.1). The boron nitride rods were used because the coefficient of expansion for the boron nitride rod is very small (0.0000002 in./in./°F).

To control the temperature inside the chamber, methanol was circulated through copper tubing coiled around the core samples (Fig. B.1). To monitor the temperatures, two thermocouple wires (copper-constantan type) were used. One wire was placed inside a 3/16-in.-diameter hole drilled into the side of the core and filled with insulation. The other wire was placed on the exterior surface of the core.

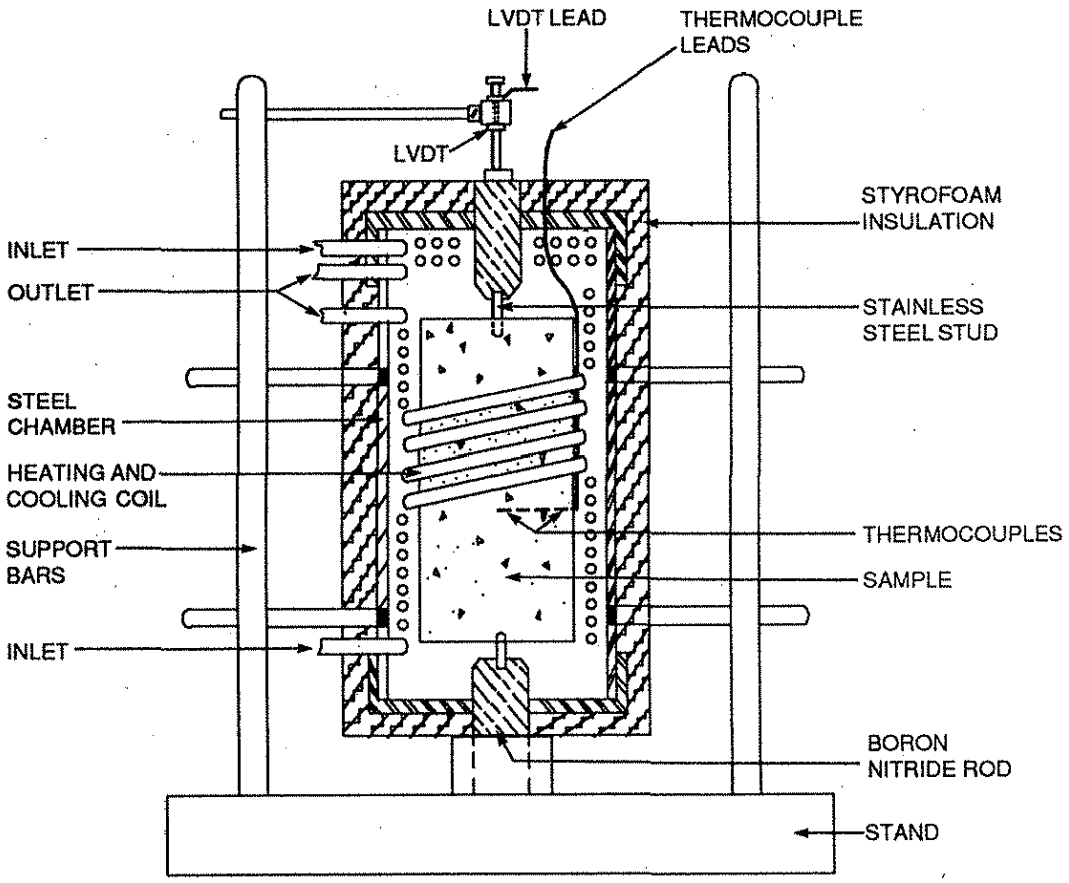

Fig. B.1. Environmental extensometer.

B.2. Test Procedures

For testing, each core was subjected to two temperature cycles, heating from 6.8° F to 140° F and cooling from 140° F to 6.8° F.

The coefficient of thermal expansion was determined by

$$\alpha = \frac{\Delta L}{\Delta T L_c} \tag{B.1}$$

in which L_c represents the original length of the core, ΔL is the change in length, and ΔT is the corresponding change in temperature. Figures B.2 and B.3 show the coefficient of thermal expansion versus time for the heating and cooling cycles, respectively, for the Boone River Bridge cores. Figures B.4 and B.5 show the coefficient of expansion for the heating and cooling cycles, respectively, for the Maple River Bridge cores. The stabilized values presented in Table 2.1 are obtained from the horizontal portion of these curves.

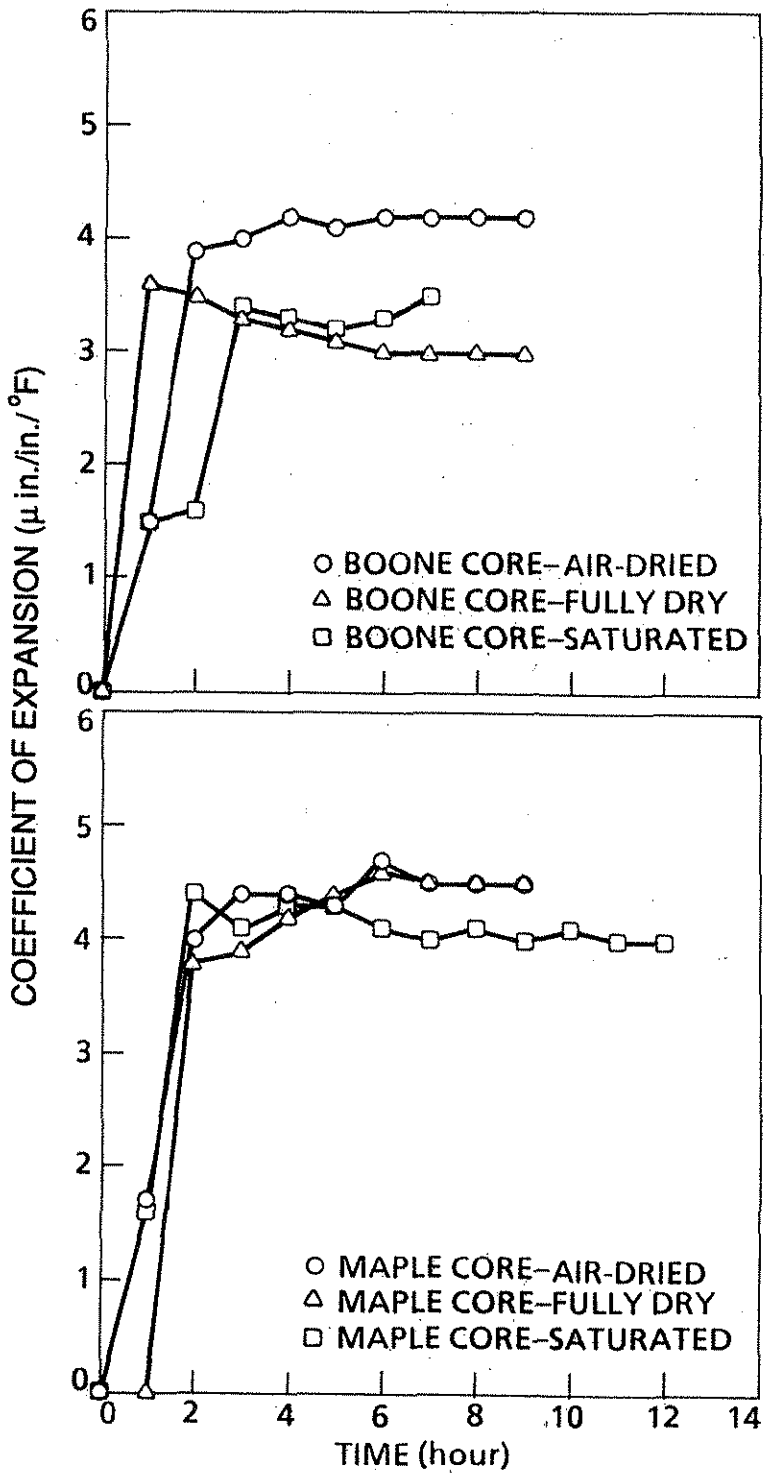

Fig. B.2 (upper). Coefficient of expansion: Boone River Bridge, heating cycle.

Fig. B.3 (lower). Coefficient of expansion: Maple River Bridge, heating cycle.

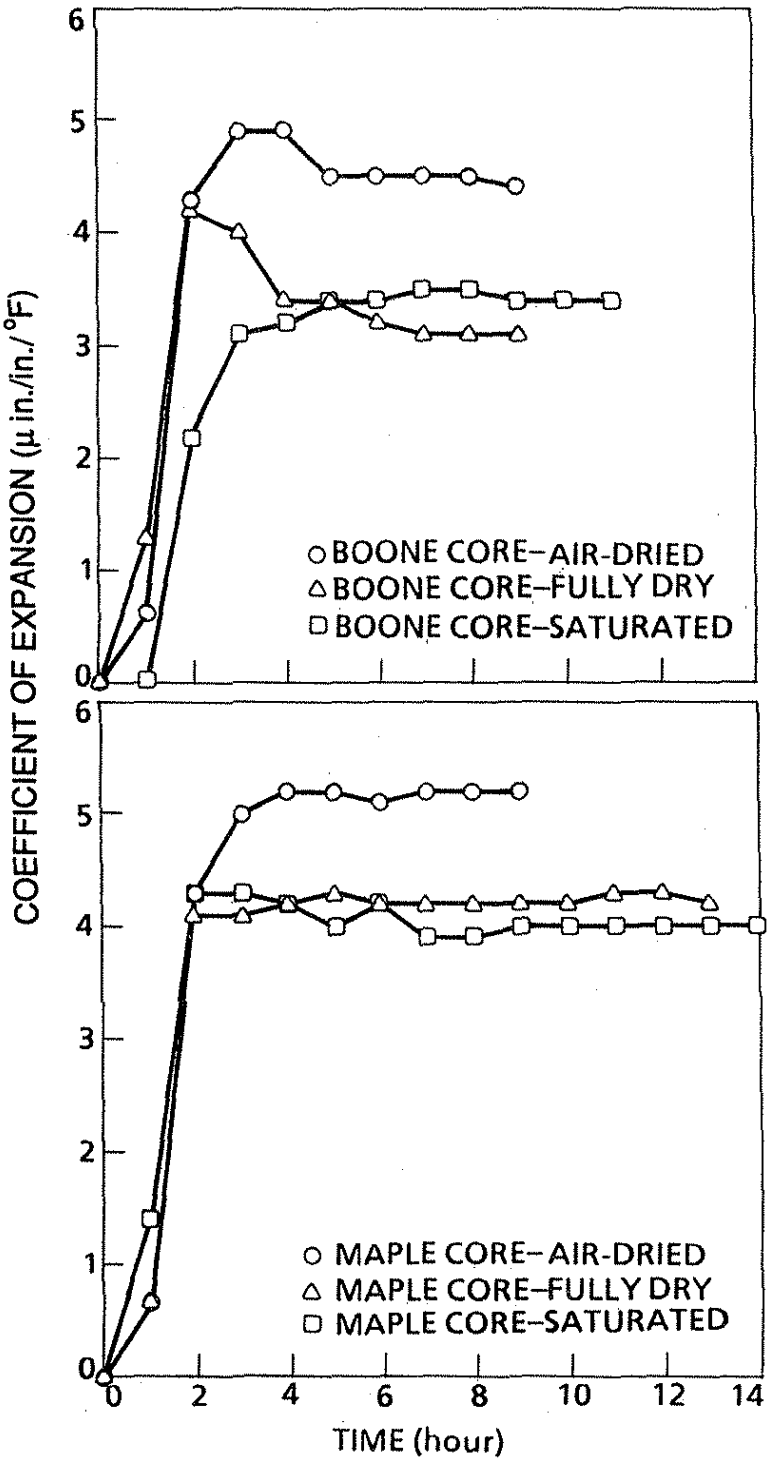

Fig. B.4 (upper). Coefficient of expansion: Boone River Bridge, cooling cycle.

Fig. B. 5 (lower). Coefficient of expansion: Maple River Bridge, cooling cycle.

APPENDIX C: EQUIVALENT CANTILEVERED LENGTH

C.1. Fixed-Head Pile with Constant k_h

For piles in a soil strata with a constant k_h, Eq. (4.1) is used to find the critical length parameter, ℓ_c, directly. From Fig. C.1 (adapted from Ref. [1]), the length of pile above the soil surface, ℓ_u, and the critical length parameter are used to find an equivalent embedded length, ℓ_e, of the equivalent cantilever. Figure C.1 is a nondimensional plot for fixed-head piles embedded in uniform soils. To use these plots, one enters the horizontal axis with the ratio of ℓ_u to ℓ_c and obtains the ratio of the equivalent embedded length, ℓ_e to ℓ_c, from the vertical axis. As explained in Sec. 4.4, lengths are given for three cantilevered equivalencies: horizontal stiffness (H), maximum moment (M), and elastic pile buckling (B). The total equivalent cantilevered lengths, L_H, L_M, and L_B, are determined by adding the equivalent embedded lengths, ℓ_{eh}, ℓ_{em}, and ℓ_{eb}, respectively, to the length of pile above the ground, ℓ_u.

C.2. Fixed-Head Pile with Varying k_h

To determine the equivalent cantilevered lengths of piles embedded in soils for which k_h varies with depth, an effective soil stiffness, k_e, should be determined. The procedure to determine the effective soil stiffness is repeated from Ref. [1].

Step 1. Guess k_e.

Step 2. Calculate $\ell_o = 2\sqrt{EI/k_e}$.

Step 3. Calculate I_k = second moment of the k_h vs. depth plot about the baseline at ℓ_o (Fig. C.2).

Step 4. Determine a new $k_e = 3(I_k)/\ell_o^3$

Step 5. Return to Step 2 until convergence.

After determining an effective soil stiffness, Eq. (4.1) is used to obtain the critical length parameter, ℓ_c. The procedure to determine the equivalent cantilevered lengths, L_H, L_M, and L_B, is the same as for a pile embedded in a uniform soil.

C.3. Example

An example is presented here to demonstrate the method of determining the equivalent soil stiffness and equivalent cantilevered lengths, L_{Hy}, L_{My}, and L_{By}, for weak axis bending of

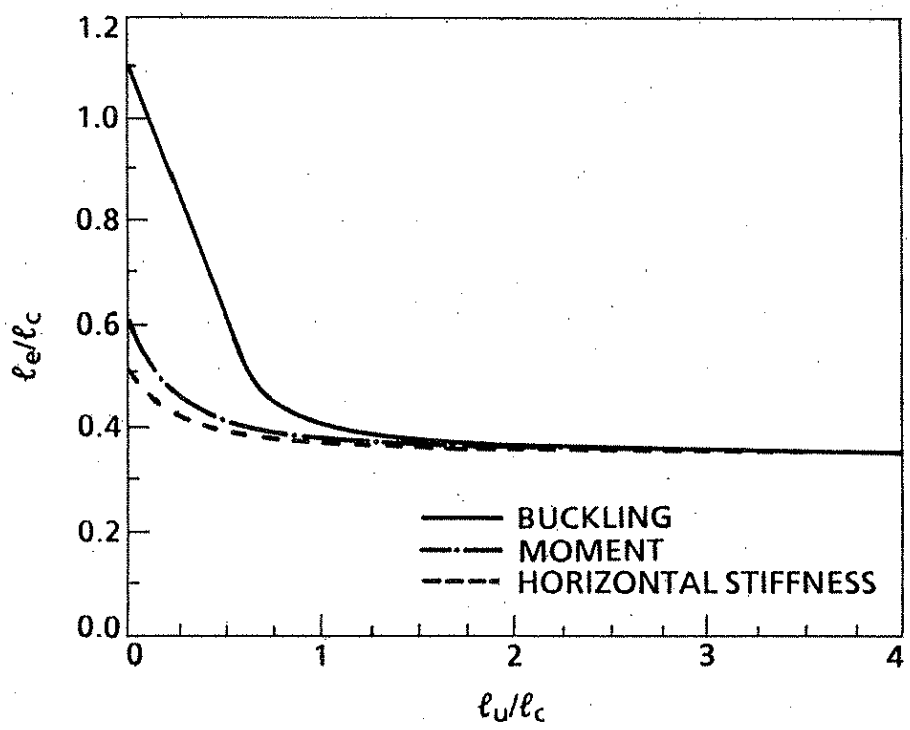

Fig. C.1. Equivalent cantilevers for fixed-head piles embedded in uniform soil.

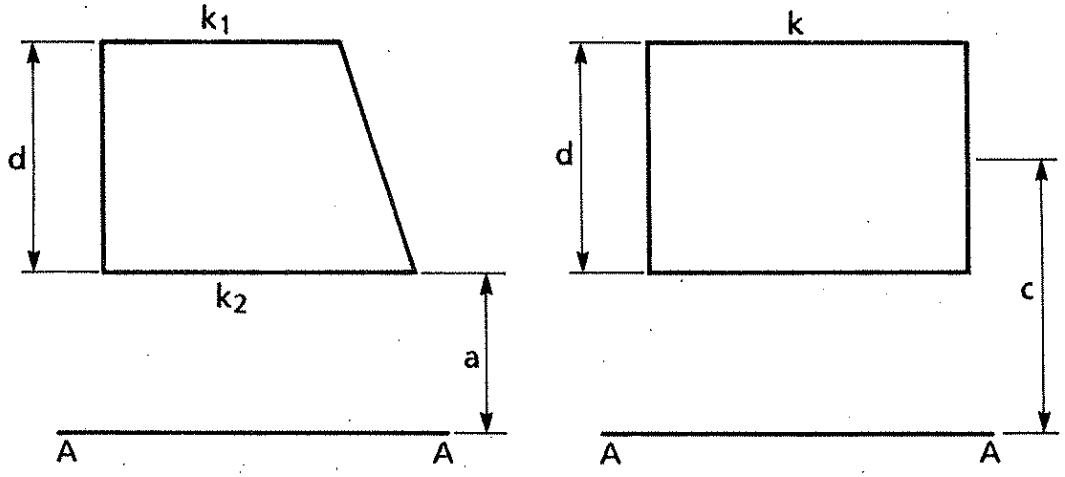

$$I_k = k_1\left[\frac{d^3}{36} + \frac{d}{2}\left(a + \frac{2d}{3}\right)^2\right] + k_2\left[\frac{d^3}{36} + \frac{d}{2}\left(a + \frac{d}{3}\right)^2\right]$$

$$I_k = k\left[\frac{d^3}{12} + dc^2\right]$$

Fig. C.2. Second moment of area about line A-A.

the piles at the Boone River Bridge. Figures 4.2a and 4.2b show the abutment-pile cross section and the stiffness, k_h, versus depth. Only the distribution illustrated in Fig. C.3 will be used in this example. The soil idealization for the predrilled hole region is certainly subjective. The length ℓ_u equals 3 ft, I_y equals 71.7 in.^{4}, and E equals 29,000,000 psi (EI_y = 14440 k-ft^2).

Step 1. Guess k_e = 100 ksf.

Step 2. Calculate

$$\ell_o = 2 \sqrt[4]{\frac{14440}{100}} = 6.93\ ft$$

Step 3. ℓ_2 = 0.93 ft, so from Fig. C.2 the second moment of the area about ℓ_o is

$$I_k = 90\ ksf\left[\frac{(6\ ft)^3}{36} + \frac{6\ ft}{2}\left(0.93\ ft + \frac{2(6\ ft)}{3}\right)^2\right]$$

$$+ 139\ ksf\left[\frac{(6\ ft)^3}{36} + \frac{6\ ft}{2}\left(0.93\ ft + \frac{6\ ft}{3}\right)^2\right]$$

$$+ 453\ ksf\left[\frac{(0.93\ ft)^3}{36} + \frac{0.93\ ft}{2}\left(0 + \frac{2(0.93\ ft)}{3}\right)^2\right]$$

$$+ 478\ ksf\left[\frac{(0.93\ ft)^3}{36} + \frac{0.93\ ft}{2}\left(0 + \frac{(0.93\ ft)}{3}\right)^2\right]$$

$$= 11639\ k-ft$$

Step 4. Determine $k_e = 3(11639\ \text{k-ft})/(6.93\ \text{ft})^3 = 105$ ksf

Second iteration:

Step 2. ℓ_o = 6.85 ft

Step 3. ℓ_2 = 0.85 ft

I_k = 11232 k-ft

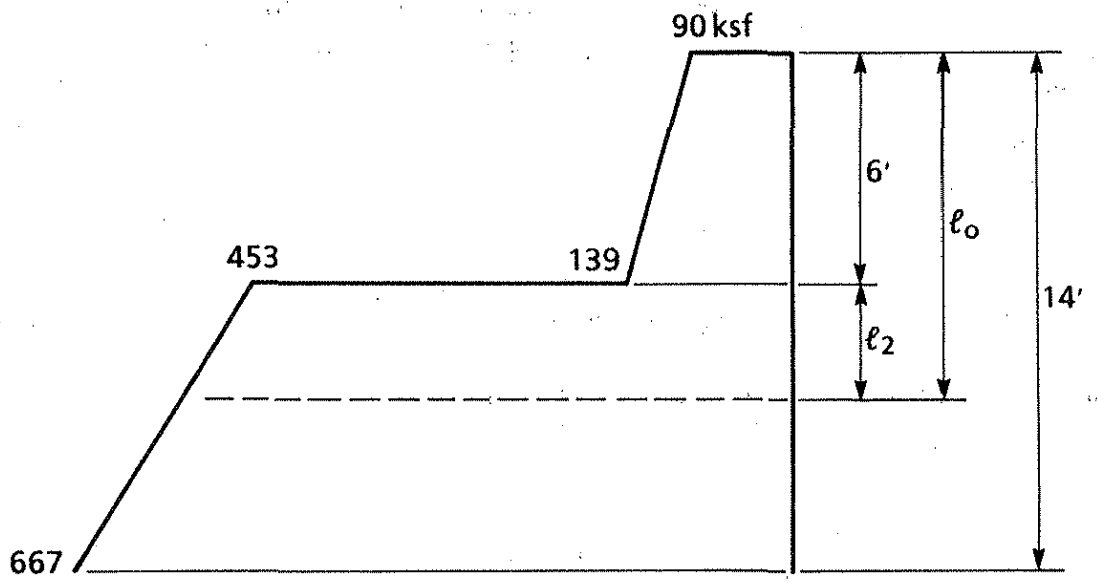

Fig. C.3. Lateral soil stiffness, k_h, for determining k_e at the Boone River Bridge.

Step 4. $k_e = 105$ ksf $= 105$ ksf

Step 5. The converged solution is $k_e = 105$ ksf

Using this soil stiffness for k_h in Eq. (4.1), the critical length parameter is

$$\ell_{cy} = 4\sqrt[4]{\frac{14440}{105}} = 13.7\ ft. \tag{C.1}$$

The equivalent embedded lengths are found from Fig. C.1 with ℓ_u/ℓ_c equal to 3 ft/13.7 ft or 0.22.

$$\ell_{ehy} = 0.43\,\ell_c = 0.43\,(13.7\ ft) = 5.9\ ft. \tag{C.2}$$

$$\ell_{emy} = 0.48\,\ell_c = 0.48\,(13.7\ ft) = 6.6\ ft. \tag{C.3}$$

$$\ell_{eby} = 0.92\,\ell_c = 0.92\,(13.7\ ft) = 12.6\ ft. \tag{C.4}$$

The total, equivalent cantilevered lengths are

$$L_{Hy} = 5.9\ ft + 3\ ft = 8.9\ ft \tag{C.5}$$

$$L_{My} = 6.6\ ft + 3\ ft = 9.6\ ft \tag{C.6}$$

$$L_{By} = 12.6\ ft + 3\ ft = 15.6\ ft \tag{C.7}$$

Table 4.3 lists the total, equivalent cantilevered lengths for the bounding soil conditions shown in Figs. 4.2b and 4.3b.

As a limiting case, the loose sand in the predrilled hole can be completely neglected. The effective soil stiffness for the sand below the level of the predrilled hole is 484 ksf. The critical length parameter, ℓ_{cy}, is 9.4 ft. The ℓ_u distance is the depth of the predrilled hole (9 ft). From Fig. C.1, with ℓ_u/ℓ_{cy} equal to 9 ft/9.4 ft or 0.96, the equivalent embedded lengths are

$$\ell_{ehy} = 0.4\,\ell_{cy} = 0.4\,(9.4\,ft) = 3.8\,ft \tag{C.8}$$

$$\ell_{emy} = 0.4\,\ell_{cy} = 0.4\,(9.4\,ft) = 3.8\,ft \tag{C.9}$$

$$\ell_{eby} = 0.42\,\ell_{cy} = 0.42\,(9.4\,ft) = 3.9\,ft \tag{C.10}$$

and total, equivalent cantilevered lengths for the case of no sand in the predrilled hole are

$$L_{Hy} = 3.8\,ft + 9\,ft = 12.8\,ft \tag{C.11}$$

$$L_{My} = 3.8\,ft + 9\,ft = 12.8\,ft \tag{C.12}$$

$$L_{By} = 3.9\,ft + 9\,ft = 12.9\,ft \tag{C.13}$$

The total, equivalent cantilevered lengths for weak axis bending to be used in design are the least of Eqs. (C.4) to (C.6) and Eqs. (C.10) to (C.12), or

$$L_{Hy} = 8.9\,ft\,or\,107\,in. \tag{C.14}$$

$$L_{My} = 9.6\,ft\,or\,115\,in. \tag{C.15}$$

$$L_{By} = 12.9\,ft\,or\,155\,in. \tag{C.16}$$

For strong axis bending, I_x of 210 in.^{4} would replace I_y.

Equivalent lengths are tabulated in Table 4.3.